2007

Reactive multilayer foils and their applications in joining

Xiaotun Qiu
Louisiana State University and Agricultural and Mechanical College, xqiu1@lsu.edu

REACTIVE MULTILAYER FOILS AND THEIR APPLICATIONS IN JOINING

A Thesis

Submitted to the Graduate Faculty of the
Louisiana State University and
Agricultural and Mechanical College
in partial fulfillment of the
requirements for the degree of
Master of Science in Mechanical Engineering

in

The Department of Mechanical Engineering

By
Xiaotun Qiu
B.S., Tsinghua University, Beijing, China, 2004
August, 2007

ACKNOWLEDGEMENTS

I wish to thank my advisor, Dr. Jiaping Wang, for providing me a chance to work on such an innovative project, which paved the way to build my thesis. It is such a great privilege working with her and she is such an inspiration that she got the best out of me.

I am also indebted to Dr. Laszlo Kecskes for helping me to conduct the DSC experiment for the cold rolled multilayer foils. I am very thankful to Dr. Wenjin Meng for his precious advice for my experiments.

I am sincerely thankful to Dr. Dorel Moldovan, who was a great help especially during my course work and to Dr. Sunggook Park, for his support and spending his valuable time in evaluating my thesis work.

My special thanks to Dr. Shengmin Guo, Zhaogao Luan, and Ranran Liu for all the help they provided for the simulation of the reactive joining process and the discussions we had all through my thesis work.

Finally, I also thank all my friends in and out of our lab, for their moral and technical support, without which I would not have succeeded in finishing my thesis.

TABLE OF CONTENTS

LIST OF TABLES

LIST OF FIGURES

ABSTRACT

In this study, Ni/Al multilayer foils were fabricated by a cold rolling method. A two-stage reaction process was observed in the reaction-ignition experiment. The phase formation process in the cold rolled foils was studied. The first reaction stage with a slow reaction velocity was the lateral growth of Al_3Ni phase at isolated nucleation sites and the subsequent coalescence into a continuous layer. The second reaction stage with a fast reaction velocity was the growth of the Al_3Ni layers in the direction normal to the Ni/Al interface until all Al was consumed. Afterwards, Al_3Ni reacted with the remaining Ni to form the final reaction product, AlNi. The reaction velocities of the first reaction stage for the cold rolled foils were around 7 mm/s.

Ti/Al multilayer foils were also fabricated by cold rolling to test whether this method can be extended to fabricate other metal/aluminum multilayer systems. The entire reaction process for the cold rolled Ti/Al multilayer foils was identified, which was similar to the cold rolled Ni/Al multilayer foils.

Reactive multilayer foils can be used as local heat sources to melt solder or braze layers and thus bond different components. Silicon wafers were bonded using reactive Ni/Al multilayer foils. A numerical model was developed to predict the temperature evolution during the bonding process. The simulation result showed both localized heating and rapid cooling during reactive foils joining process. Based on our experimental observation, the bonding strength of the reactive bond was estimated to

be larger than the failure strength of bulk silicon. Moreover, leakage test in isopropanol alcohol (IPA) showed that reactive foils bonds possessed good hermeticity for liquid.

1. INTRODUCTION

Combustion synthesis, also called reaction synthesis, is a process in which two or more materials with large exothermic heats of mixing, known as reactants, are combined together. When the reactants are heated sufficiently, they begin to spontaneously intermix on the atomic scale, releasing heat in the process. A large body of literature exists on this process, and it has been reviewed extensively [1-4].

In general, combustion synthesis has been accomplished using mixed reactant powders which are pressed into a pellet of certain green density (weight divided by the volume of an unreacted powder compact, which is smaller than the theoretical density of the material due to the presence of pores in the powder compact). Combustion is initiated by an external energy source to heat the compact. Once combustion begins, the energy released by intermixing contributes to increasing the local temperature, resulting in faster intermixing and combustion. A large amount of materials are reported to have been synthesized with this general method, including carbides, borides, silicides, nitrides, sulfides, hydrides, intermetallics, and complex composites. Table 1.1 lists a number of materials which can be produced by this process. Combustion synthesis has many advantages such as the ability to create high melting temperature materials in a low-temperature process, near-net form fabrication, and rapid material synthesis.

The ignition of combustion synthesis can be subdivided into two different modes. The first mode is termed self-propagating high-temperature synthesis, or SHS. In this method, the compact is heated locally using an external heat source. The local heating initiates the reaction locally, releasing heat that drives the reaction forward. The reaction moves

across the compact in a self-propagating manner, driven by its own heat. In 1960s, Russian scientists reported self-sustaining reactions in powder compacts [6]. They found that the formation of TiB_2 from Ti and B powders could produce heat fast enough to propagate as a "white solid flame" across a powder compact. They called this process self-propagating high-temperature synthesis (SHS). SHS can be used in powder compacts to join materials and produce hard compounds in near-net shapes. The other method of ignition is termed thermal explosion, or simultaneous ignition. In this method, the entire compact is heated simultaneously, for example in a furnace, until all of the reactant powder spontaneously converts into product.

Table 1.1 Some Materials Produced by Combustion Synthesis (Moore, 1995)

Borides	CrB, NbB, TiB, MoB, WB, VB
Carbides	TiC, NbC, SiC, WC, TaC, VC
Nitrides	BN, AlN, SiN, TiN, VN, TaN
Silicides	ZrSi, $NbSi_2$
Aluminides	TiAl, NiAl, CoAl, $NbAl_3$
Hydrides	ZrH_2, TiH_2, NbH_2
Composites	$TiN - Al_2O_3$, $TiC - Al_2O_3$, $TiB_2 - Al_2O_3$

However, powder compacts have several limitations when used for combustion synthesis. The density of the final product is often limited by the green density of the powder compact. If the combustion synthesis reaction is solid-state, the particles can only inter diffuse with each other where they are in physical contact. The size of the powder

particles is often large compared to the characteristic diffusion distance for a given system, making it difficult to achieve full intermixing. Particles of highly reactive components will often have a passivating outer coating that acts as a barrier to diffusion with other reactants. Moreover, voids between the powder particles limit thermal diffusion through the compact, reducing the ability of the reaction to be driven by its own heat.

With modern thin film deposition techniques, fully dense multilayer materials with similar exothermic reactions can be fabricated. Such reactive multilayer foils consist of hundreds or thousands of nanometer scale alternating layers of two or more materials, known as reactants, which can mix exothermically. When heat is applied locally to the foil, it undergoes SHS in a fashion similar to powder compacts. Structures of reactive multilayer foils offer several potential improvements over powder compacts. The individual layers in a reactive foil are usually on the scale of tens of nanometers, which significantly decreases the diffusion distances involved in interatomic diffusion between the reactants. The thickness of the individual reactant layers can be controlled during fabrication, allowing significant control over the properties of the foil. The individual layers are in intimate contact with each other, which increases both thermal and atomic diffusion in the system while also eliminating voids in the system. Moreover, having thin layers of reactants that are in intimate contact with each other makes the SHS reaction propagate faster in most reactive foils than in a powder compact with the same components.

So far, self-propagating reactions have been reported in Ti/B, Ni/Si, Zr/Si, Rh/Si, Ni/Al, Monel (7Ni:3Cu)/Al, Ti/Al, Pd/Al, Pt/Al, and CuO_x/Al multilayer materials [9-16]. The driving force for self-propagating formation reactions is the reduction in chemical bond energy. In an A-B multilayer system, when one end of the foil is ignited with a small thermal pulse (such as a spark) at room temperature, local atoms will diffuse normal to the layers with A-A and B-B bonds being exchanged for A-B bonds, as shown in Figure 1.1. In this process, heat is released and conducted parallel to the layers. If atomic diffusion and energy release are sufficiently fast, then the reactions are self-propagating. These reactions can travel as fast as 25 m/s and can reach temperatures above 1500 ^{o}C.

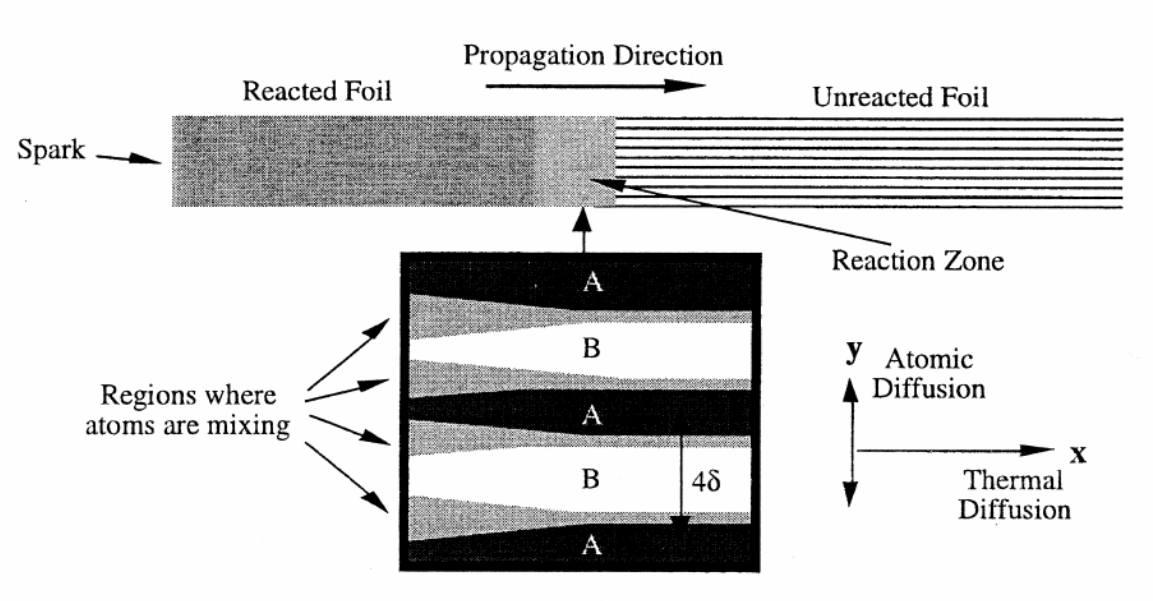

Figure 1.1 Schematic illustration of a self-propagating reaction in a multilayer foil with bilayer period 4δ. A spark is used to ignite one end of the foil and then a thin reaction zone propagates along the *x*-direction into the unreacted foil. An expanded view of the reaction zone shows the growth of the intermixed region between A and B as the reaction traverses the foil [9]

Reactive multilayer materials are most commonly fabricated using physical vapor deposition (PVD) methods such as magnetron sputtering and electron-beam evaporation,

and occasionally via mechanical techniques such as repeated rolling of layered composites. The PVD methods involve creating a vapor of a material, known as the source material, and then depositing the vapor onto a substrate. The rate at which the vapor is deposited is controllable, allowing the growth of layers with thickness ranging from nanometers to micrometers. One way to generate chemically distinct layers is to co-deposit the materials where several sources are directed to one substrate and atomic fluxes from each source are shuttered to create the alternate layers. Another way is to rotate the substrate over several sources to deposit the alternate layers. Most of the reactive multilayers have been deposited onto substrates such as Si, glass, or photoresist. They possess nanoscale layers and usually have atomic intermixing between the individual layers, which occurs during deposition, to some extent. The alternative layers in metal/metal systems such as aluminides are typically polycrystalline. The layers have standard growth textures and in plain grain size tends to scale with layer thickness. An intermixed layer often grows between the two polycrystalline layers.

Alternatively, multilayer foils can also be made by cold rolling. Battezzati *et al* fabricated Ni/Al multilayer foils with overall composition $Al_{50}Ni_{50}$ by rolling a square multilayer composite of Ni and Al in a folded stainless steel sheet that was previously hardened by repeated rolling. They kept the opening between the rollers constant at a value for which the thickness of the composite was halved after rolling in two perpendicular directions. This was defined as a rolling pass. After every pass the folder was opened and the multilayer was folded once to recover the original thickness and used in the next rolling pass. Sieber *et al* fabricated Ni/Al multilayer foils by a fold and roll method. A multilayer sandwich of Ni and Al was rolled in a manual rolling machine at a strain rate of 0.1 S^{-1} to

a thickness of about 80 μm to obtain the starting material. Subsequently, the starting material was folded to double the thickness and rolled to 80 μm in 10 cycles. Then the above fold and roll cycle to 80 μm was repeated several times to get the final multilayers. The cold rolled foils made by both methods were used to study the solid state reactions in Ni/Al multilayers during annealing.

To ignite self-propagating reactions in reactive multilayers, several different methods have been employed. Generally, the reactions are started by pulsing one end of a sample with a small burst of energy. The energy can be applied using the impact from a sharp stylus, a spark from an electrical source, heat from a filament, or radiation from a laser beam. Once the reaction is started, the speeds at which they propagate can be characterized using different measurement methods. Reiss *et al* used a photodiode and a simple optical system to measure the reaction velocities of the reactive foils (Figure 1.2) [22]. The velocities of the self-propagating formation reactions were measured using visible radiation emitted by the foils during the reaction. The foils were ignited at one end by a spark. As the reactions propagated down the foils, emitted light was collected by a linear array of fibers with known spacing that were separated from the foils by a thin piece of glass. The light from the fibers was directed onto a Si PIN photodiode whose output was recorded by a digital oscilloscope. Once a foil was ignited and the emitted light was collected as a step trace, the velocity of the self-propagating reaction was determined by finding the time between steps.

High speed cameras have also been used to capture reaction fronts traveling along the reactive foils. Adams *et al* used a high speed camera that aligned perpendicular to the

direction of flame propagation to measure the reaction velocities of AlPt thin films (Figure 1.3) [15]. The camera with eight 576×385 charge coupled devices was configured with a strobe lamp, a timer, and electronics so that propagating reactions could be viewed in the plane of substrates. The typical frame capture times were 20 ns with all images of a single propagation event captured within a single strobe pulse. The interframe time range was 0 - 1 ms. Average propagation speed was determined from up to eight possible photographs.

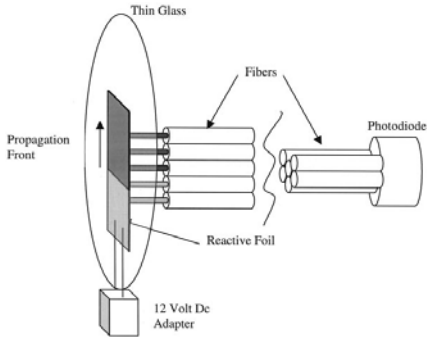

Figure 1.2 Schematic diagram showing the measurement of reaction velocities. The reaction is started with a small spark and its passage is recorded using a fiber array, a photodiode and an oscilloscope [22]

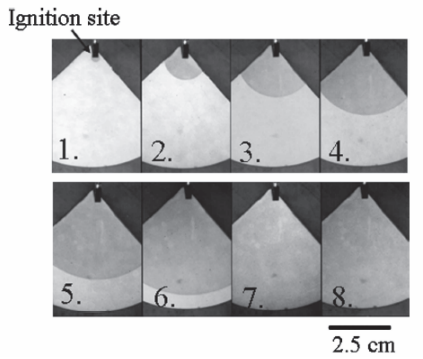

Figure 1.3 High speed photographs showing a self-propagating high temperature reaction in an Al/Pt multilayer thin film. Light-colored portion of film is unreacted multilayer. Speed of expanding wavefront is 59 m/s [15]

Numerous studies of interface reactions have been performed in different multilayer systems. A common feature of these multilayers is the apparently large free energy, typically several tens of kJ/mol, available for phase formation. This leads one to conclude that all possible product phases should be able to form from the very beginning of the reaction. However, numerous studies of metal/aluminum and other systems have shown that phases form sequentially and not simultaneously [25, 34]. Furthermore, recent investigations of Nb/Al [40], Ni/Al [34], and Ti/Al [48] multilayers have demonstrated the significance of nucleation kinetics, and hence nucleation barriers, in product phase formation. In the light of this increasing complexity of processes associated with reactive phase formation in multilayers, it is not surprising to find mounting evidence for differences in behavior depending on the method of fabrication of the multilayers.

Reactions in the Ni/Al multilayer system have been extensively characterized. The Ni/Al phase diagram shows that four intermetallic phases (Al_3Ni, Al_3Ni_2, AlNi and $AlNi_3$) can be formed [33]. The studies prior to 1990 were summarized in a review by Colgan [33] and showed that Al_3Ni was the first phase to form.

For the PVD multilayers, studies by Ma *et al* [34] and Edelstein *et al* [35] included calorimetric measurements on Ni/Al multilayer films prepared by electron-beam evaporation and by ion beam deposition, respectively. Ma *et al* demonstrated that Al_3Ni was the first phase to form, but that the nucleation and growth to coalescence of the first layer of this phase was kinetically separated from the following growth stage, giving rise to two separate calorimetric peaks, although only a single product phase was formed. Similar results were also obtained by Barmak *et al* using sputtered Ni/Al multilayer films

[39] and by Qiu *et al* using cold rolled Ni/Al multilayer foils [79]. The observation of the first nucleation and growth peak was indicative of the presence of nucleation barriers to the formation of this phase and was in disagreement with the nominally large driving force for the reaction, i.e., the large heat of formation of this phase. Large driving forces imply that nucleation barriers should be negligible; hence, only one calorimetric peak should be observed for any one phase. These results indicated that the effective driving force for phase formation must be considerably smaller than the bulk heat of formation of the product phase. Possible sources of this reduction in driving force are reactions which may precede the formation of any new phase. Ma *et al* attempted to investigate the processes preceding Al_3Ni formation, and found that the Ni and Al composition profiles broadened upon annealing to a stage prior to Al_3Ni nucleation, indicating that interdiffusion had taken place. They interpreted that the interdiffused region was mainly composed of solid solutions. Edelstein *et al* found that the first phase to form can be AlNi, Al_3Ni or Al_9Ni_2, depending on the overall stoichiometry and the modulation period of the multilayers. Barmak and co-workers found that B2 AlNi phase and an amorphous phase were formed during deposition of the multilayers made by magnetron sputtering, which considerably reduced the driving force for subsequent reactions. Depending on the periodicity of the multilayers, the formation of Al_3Ni or Al_9Ni_2 followed by Al_3Ni was observed. In the work of Blobaum *et al* [37], Al_9Ni_2 was the first phase to form in a series of Ni/Al multilayers except for very small bilayer period (12.5 nm), in which Al_3Ni was the first phase observed. In contrast to the Ni/Al multilayers made by physical vapor deposition methods, which showed different behaviors for the formation of the first phase, in the cold rolled Ni/Al multilayer foils, Battezzati [19], Sieber [20] and Qiu [79] all

demonstrated that the first detectable phase to form was Al_3Ni. And more recent work done by Sauvage *et al* [51] on cold rolled Ni/Al multilayers revealed that during the severe plastic deformation process metastable or non-equilibrium solid solutions with various compositions were formed prior to the formation of any new phase.

When a particular multilayer sample reacts to form a compound, the heat released can be measured using differential scanning calorimetry (DSC) [23]. In each DSC run, about 7-10 mg multilayer foil was heated from 50 ^{o}C to 725 ^{o}C at a rate of 40 ^{o}C /min in flowing Ar. A base line was obtained by repeating the heating cycle, which was then subtracted from the heat flow in the first run. By integrating the net heat flow with respect to time, the heat of reaction was obtained. Wang *et al* measured the heat of reaction for Ni/Al multilayer foils with different bilayer thickness. They found that the heat of reaction decreased as the bilayer thickness decreased. This indicated that the volume percentage of intermixing between layers, which occurred during the deposition, was significant and led to heat losses, and consequently a reduction in the measured heats of reaction. They suggested a formula to calculate the heat of reaction for the Ni/Al multilayer foils with different bilayer thickness.

$$\Delta H = \Delta H_o \left(1 - \frac{2\omega}{\lambda} \right) \tag{1}$$

In the equation above, ΔH_o is the enthalpy of formation for the compound that is produced, ω is the intermixing thickness and λ is the bilayer thickness. Using the measured heat of reactions, it was estimated that ω was 2.3 ± 0.3 nm and the maximum heat of reaction, ΔH_o, was 1268 ± 21 J/g for Ni/Al multilayer foils.

With large heats of reaction, self-propagating reactions in multilayer foils offer a new method to dramatically improve soldering and brazing technologies by using the foils as local heat sources to melt solder or braze layers and thereby join components, as shown schematically in Figure (1.4). This process eliminates the need for furnaces or other external heat sources, and with much localized heating, temperature sensitive components can be joined without thermal damage. It is also advantageous for joining materials with very different coefficients of thermal expansion, such as joining metals and ceramics. The rapid nature of the process eliminates oxidation of the molten solder or braze and the very limited heating of the components dramatically reduces thermal stress in the components being bonded. Reactive foil soldering or brazing can be performed at room temperature in various environments, such as in air or vacuum.

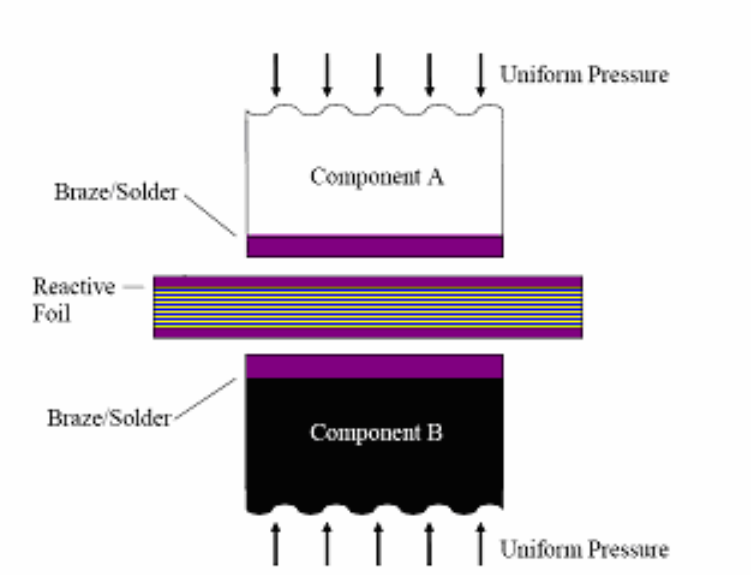

Figure 1.4 Cross-sectional schematic of reactive foil joining. Uniform pressure is applied to components A and B before igniting the reactive foil. The heat released by the reacting foil melts solder or braze layers on components A and B. The amount of heat released is limited, so the bulks of components A and B are not heated significantly.

Wang *et al* joined Ni/Au coated stainless steel specimens with AuSn solder using reactive nanofoils as local heat sources, under an applied pressure of as low as 10 kPa [23, 29]. Multilayered Ni/Al nanofoils were made by magnetron sputtering and the total thickness of the foil ranged from 40 to 180 μ m. Heat generated by the reaction of the nanofoil completely melted the AuSn solder layers and bonded the components. The microstructure of the AuSn solder layer consisted of a very fine lamellar eutectic structure, with a light Au rich phase and a dark Sn rich phase (Figure 1.5).

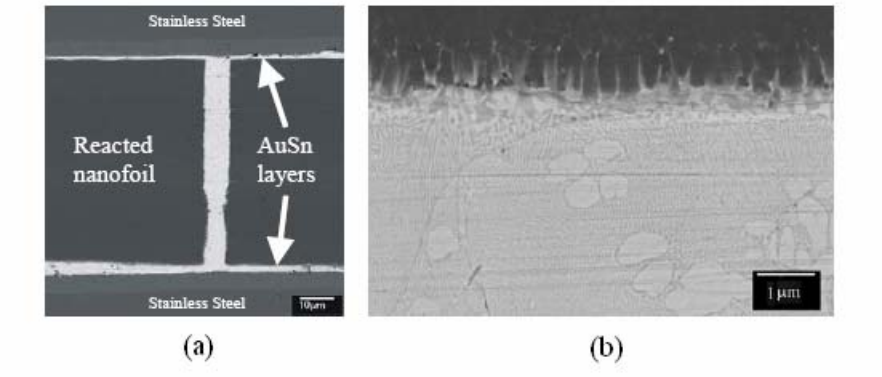

Figure 1.5 Joining stainless steel specimens using reactive nanofoils and solder/braze layers: (a) a cross-sectional SEM micrograph of two stainless steel specimens joined using a Ni/Al nanofoil and two AuSn solder layers; (b) nanoscale lamellar eutectic structure of the AuSn solder layer after reactive joining [23]

The stainless steel reactive joints were tested in tension at room temperature and the shear strengths of joints were plotted as a function of foil thickness in Figure 1.6. The joint made with the thinnest foil (23 μm) showed a shear strength of only 2 MPa. Thicker foils can increase the available energy, enhance wetting, and improve the strength of the joints, until a critical thickness of 40 μm was reached. Above 40 μm the shear strength of the stainless steel joints was constant around 48 MPa, compared to 38 MPa for conventional solder joints. The higher strengths in the reactive joints were attributed to the refined AuSn microstructures that developed during rapid cooling.

A numerical study was performed to predict the amount and duration of the melting of solder layers as the nanofoil thickness was varied. The predictions of the melting of the AuSn solder layers during reactive joining of stainless steel as a function of the thickness of the Ni/Al foils showed that the amount of AuSn solder that melted increased as foil thickness increased (Figure 1.7). The length of the period during which the whole AuSn solder layer was molten also increased with increasing foil thickness.

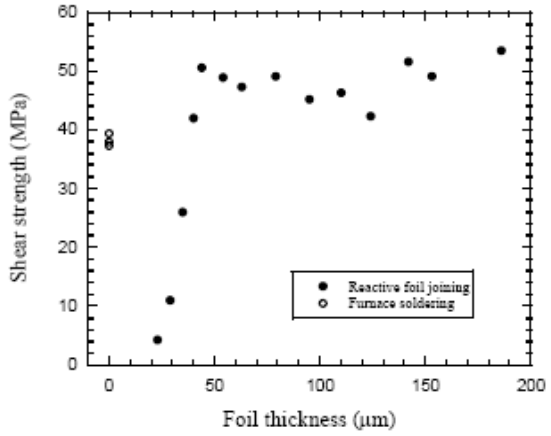

Figure 1.6 Shear strength of stainless steel reactive nanofoil joints as a function of foil thickness [23]

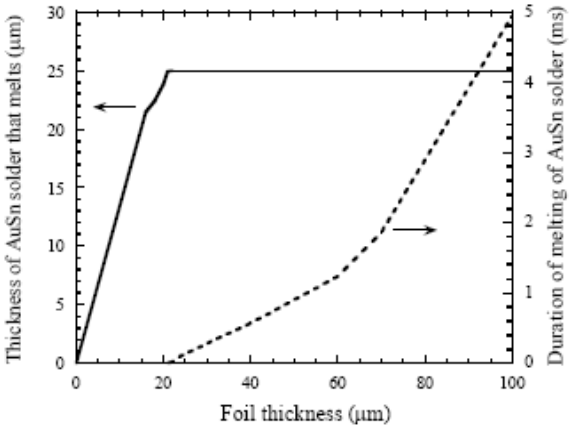

Figure 1.7 Numerical predictions of the thickness of AuSn solder that melts and the duration of the melting at the interface between solder and stainless steel specimens, as a function of foil thickness [23]

Numerical predictions of the temperature profiles during the reactive joining showed that the temperatures in the joining area decreased very quickly after reaction and that the heat effected zone in the stainless steel samples was very limited (Figure 1.8). In stainless steel, at 100 μm from the interface between the solder layer and the stainless steel, temperature decreased to 60 °C within 0.2s following reaction, showing that the heat exposure to the stainless steel components was very limited and localized, which was in agreement with the experimental measurements using an infrared camera. Both numerical predictions and infrared camera measurements demonstrated the rapid cooling and limited and localized heating of components during reactive nanofoil joining.

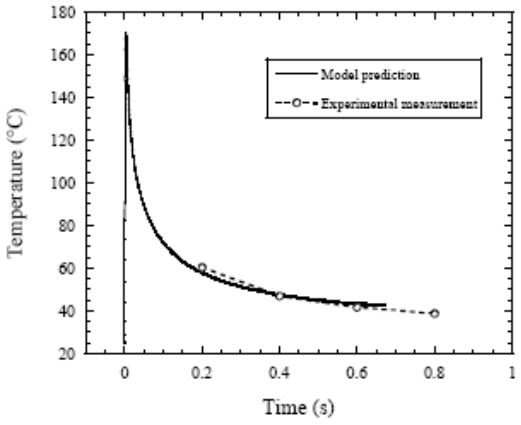

Figure 1.8 Numerical predictions and experimental measurements of temperature changes in stainless steel at 100 μm from the solder/stainless steel interface [23]

Other materials such as Al-Al, Ti-Ti, metallic glass-metallic glass and Cu-Si have also been successfully joined using reactive nanofoil joining method.

Namazu *et al* used Ni/Al multilayer film to join MEMS (Microelectromechanical Systems) elements [32]. They addressed reactive film soldering between glass and silicon elements. Process flow for fabricating AuSn film soldering of glass and silicon is shown

in Figure 1.9. A lift-off method was used to pattern the AuSn solder and the Ni/Al film. With inducing spark by electrode contact just above the Ni/Al reactive film, the film was ignited. The solder was melt by the local heating with exothermic reaction in the reactive film, and consequently joined glass-silicon wafer elements (Figure 1.10).

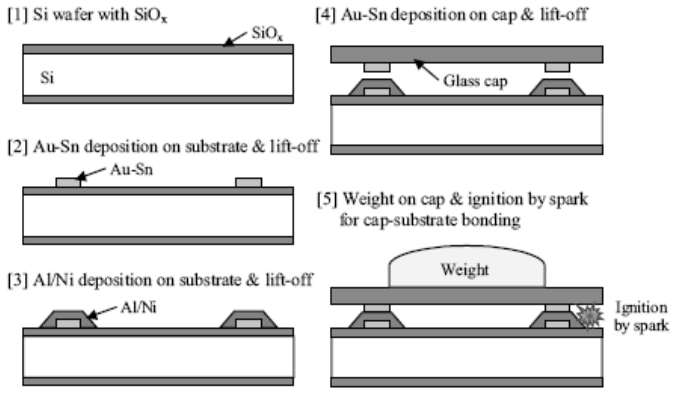

Figure 1.9 Fabrication process of MEMS solder bonding chip [32]

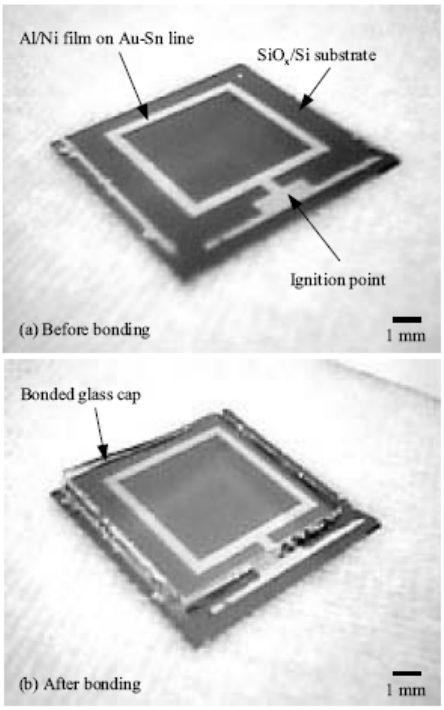

Figure 1.10 Photographs of bonded glass-silicon elements. The bonding was achieved by using AuSn solder and Ni/Al reactive film [32]

The present work focuses on reactive multilayer foils and their applications in joining.

The objectives of the present research are:

(i) to fabricate reactive multilayer foils by cold rolling;

(ii) to bond silicon wafers using reactive multilayer foils;

(iii) to simulate the temperature evolution during the bonding process.

2. EXOTHERMIC REACTIONS IN COLD ROLLED NI/AL REACTIVE MULTILAYER FOILS

Thin film reactions in the Ni-Al system have been extensively characterized. Previous studies of a number of metal/aluminum systems, such as Nb/Al and Ni/Al, showed that during the formation of the Al rich phase a nucleation and growth event occurred prior to the subsequent thickening of the product phase. In this case, phase formation became a two-stage process although only a single-product phase was formed, based on the model of Coffey *et al* [40]. The interpretation of this two-stage process is that during stage one the product phase nucleates at isolated positions in the interface and grows predominately in the plane of the interface and subsequently coalesces into a continuous layer. This stage can be modeled using nucleation-and-growth kinetics. Stage two is the subsequent thickening of this contiguous layer in the direction perpendicular to the interface, a process that can be modeled using one-dimensional diffusion-controlled growth kinetics. This two-stage formation process was used to explain the two exothermic peaks that were observed for the formation of a single phase in differential scanning calorimeter (DSC) runs of reactive multilayer thin films.

Lucadamo *et al* presented another proof for this two-stage formation process [50]. They used in situ x-ray diffraction experiments with high-intensity synchrotron radiation to detect Al_3Nb at the onset of the reaction in Nb/Al multilayer thin films. They observed two discrete increases in the measured Al_3Nb peak intensity during the reaction, indicating a two-stage formation mechanism analogous to the results of the double peaked DSC data.

However, this two-stage formation process has not been directly observed in multilayer thin films. Ma *et al* observed a continuous Al_3Ni layer (about 15 nm thick) in the Ni/Al multilayer film annealed to 550 K (temperature above the first peak in the DSC curve for Ni/Al multilayer thin films). But they failed to reveal the presence of Al_3Ni at the interface at 525 K (up-ramp of the first peak in the DSC curve for Ni/Al multilayer thin films), since Al_3Ni formed most likely at isolated points and hence was not easily resolvable from the rest of the interdiffused region. Meanwhile, the bilayer thicknesses of multilayer thin films are in the 10's of nm range and the self-propagating reaction in these films can complete in only several milliseconds. So the two-stage formation process has not been directly observed in multilayer thin films during the self-propagating reactions.

In this study, Ni/Al multilayer foils were fabricated by a cold rolling method. The cold rolled foils possessed alternating layers of Ni and Al with thicknesses in the range of micrometers. With much bigger bilayer thickness and much slower reaction velocity, the cold rolled foils could reveal the details of the exothermic formation process.

2.1 Fabrication of the Cold Rolled Ni/Al Multilayer Foils

Ni/Al multilayer foils were fabricated by a cold rolling method using a laboratory rolling mill with roller diameter of 65 mm.

Figure 2.1 shows the schematic of the cold rolling procedure. Thin sheets (3 inch by 3 inch square) of pure elements of Ni and Al with initial thickness of 25.4 μm and 38.1μm, respectively (McMaster-Carr Company, Ni minimum purity of 99.6 wt % , Al minimum purity of 99 wt %) were alternatively stacked together in order to obtain a 1/1 atomic

ratio of Ni/Al. The stacked sheets were then rolled to form a tube. Two tubes were made at the same time with the same number of Ni/Al layers. One of them had Ni as the outer layer while the other had Al as the outer layer. These two tubes were flattened by a vise, put in a folded stainless steel sheet previously hardened by repeated rolling, and cold rolled a few times to reduce the thickness to half of their original thickness. Afterwards, they were taken out of the stainless steel sheet and stacked together to recover the original thickness. In this way, two same metal layers would not become layered side by side in the final multilayer foils. The stacked foils were then cold rolled without changing the distance between the rollers. The thickness of the foil was reduced to half in one rolling pass. Subsequently, the resulting foils were cut into halves, stacked together, and the rolling procedure mentioned above was repeated for several times until a uniform multilayer foil was achieved. The total thickness of the foil was around 200 μm.

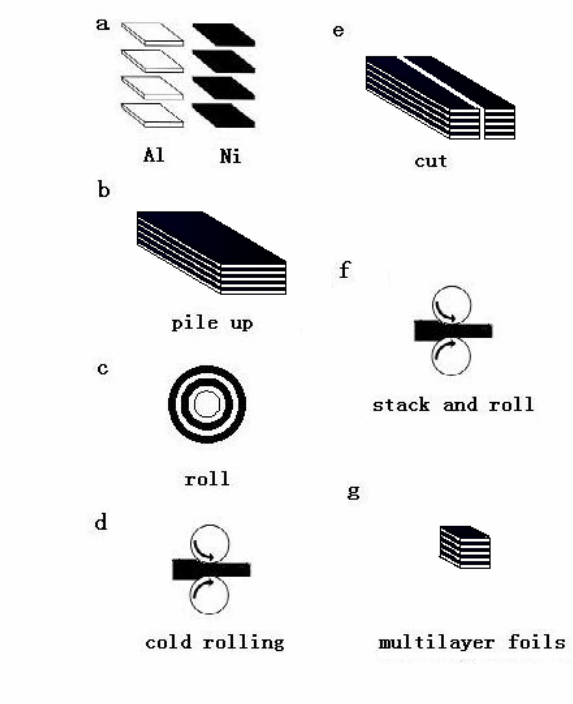

Figure 2.1 Schematic of the cold rolling procedure.

2.2 Ignition of the Cold Rolled Ni/Al Multilayer Foils

The cold rolled Ni/Al multilayer foils were ignited by a flame. After heating for several seconds, a self-propagating reaction started in the foil and two distinct reaction steps were observed. At the step one, the reaction spread along the direction parallel to the surface of the foil at a relatively slow rate and the foil surface became darker. Then at the step two, the reaction propagated at a much higher speed, released a large amount of heat and showed visible red light.

2.3 Characterization of the Cold Rolled Ni/Al Multilayer Foils

2.3.1 XRD Experiment

To characterize the reaction products, reacted Ni/Al foils were ground into powders for symmetric X-ray diffraction (XRD) examination using Cu $K\alpha$ radiation. As cold rolled Ni/Al foils were also examined by XRD for comparison. XRD traces for as cold rolled and reacted Ni/Al multilayer foils are plotted in Figure 2.2. For the as cold rolled foils, all the peaks in the x-ray diffraction scan correspond to Al and Ni, as shown in the upper scan in Figure 2.2. After reaction, all major peaks correspond to the ordered B2 AlNi compound, which is the equilibrium compound for this composition, as shown in the lower scan in Figure 2.2.

A PVD foil (made by magnetron sputtering) was also ignited and characterized by XRD in comparison with the cold rolled foil, as shown in Figure 2.3. For the unreacted foils, the trace for the PVD foil contains only four Ni and Al Bragg reflection peaks (Al (111), (222) and Ni (111), (222)), while the trace for the cold rolled foil contains reflections of most of Ni and Al crystal orientations. However, the traces of the reaction products are

the same for both the cold rolled and the PVD foils, which is the ordered B2 AlNi compound.

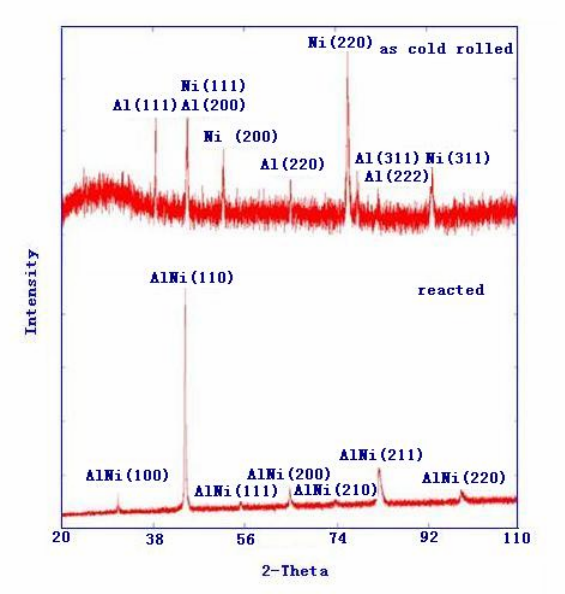

Figure 2.2 XRD patterns of cold rolled Ni/Al multilayer foils before and after reaction.

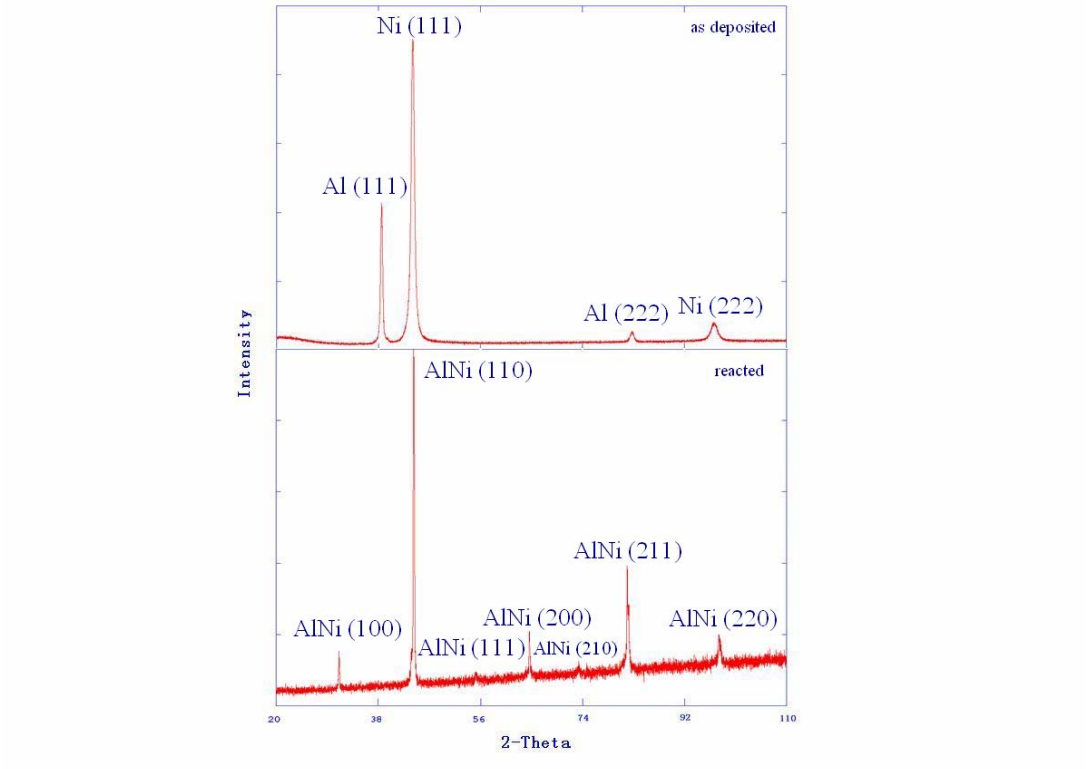

Figure 2.3 XRD patterns of PVD Ni/Al multilayer foils before and after reaction.

2.3.2 SEM Experiment

Cross sections of as cold rolled and reacted foils were polished and then characterized using a Hitachi S-3600N scanning electron microscope (SEM) with energy dispersive X-ray Analysis (EDX). Figure 2.4 shows SEM images of an as cold rolled Ni/Al multilayer foil and a reacted foil. No sign of reaction can be observed in the cold rolled Ni/Al multilayer foil. Necked Ni particles are embedded in the Al matrix and aligned along the rolling direction. Most of the Ni particles possess a wavy surface. No initial intermixing layers can be identified at the Ni/Al interfaces, which is different from the PVD foils. In the PVD foils, phase formation was observed to start during the deposition, with the B2 AlNi phase as a reaction product. The average bilayer thickness is in the range of several micrometers which is much thicker than most PVD foils that typically have bilayer thicknesses in the range of tens of nanometers. Two phases can be observed in the reacted foil: AlNi as the reaction product and some remaining unreacted Ni. There are also some pores in the reacted foil, which result from contraction during rapid cooling and density increase during the reaction.

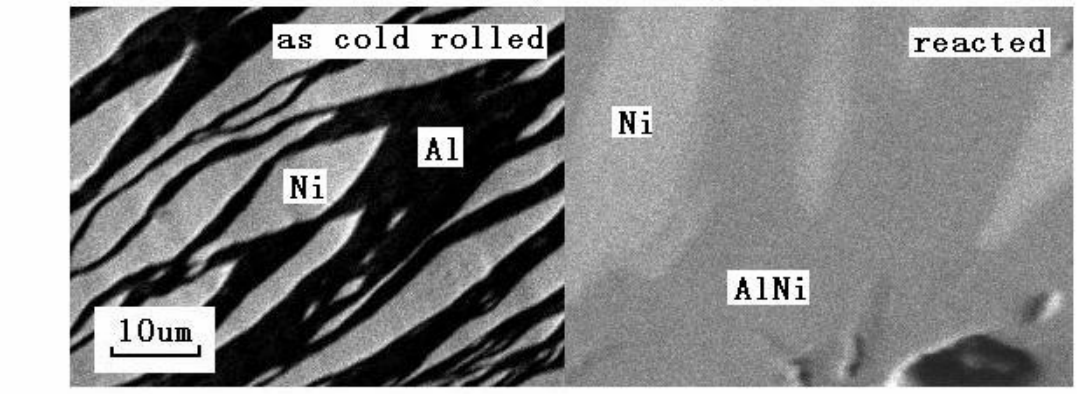

Figure 2.4 SEM images of a cold rolled Ni/Al multilayer foil and its reaction product.

The reacted foil was etched by electropolishing to reveal the grain boundaries, where the reacted foil was used as the anode and a graphite bar was used as the cathode. The electrolyte was a mixture of 80% acetic acid and 70% perchloric acid with a volume ratio of 9/1. The electropolishing process was conducted under a voltage of 20V at room temperature for 10 minutes. Figure 2.5 shows a SEM image of an electropolished reacted foil. The average grain size was estimated to be around 15 micrometers.

2.3.3 DSC Experiment

The reaction process was analyzed using a Perkin Elmer differential scanning calorimeter (DSC7). In each DSC run, about 10 mg multilayer foils were heated from 200 ^{o}C to 725 ^{o}C at a rate of 40 ^{o}C /min in flowing N_2. A base line was obtained by repeating the heating cycle, which was then subtracted from the heat flow data obtained in the first run. By integrating the net heat flow with respect to time, the heat of reaction was obtained.

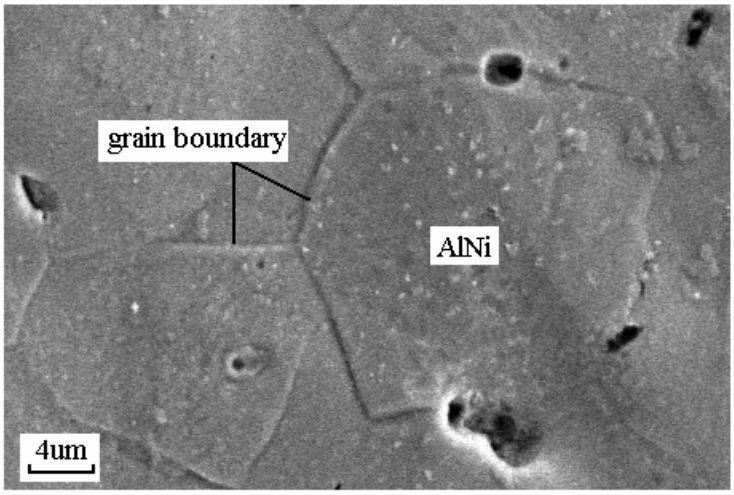

Figure 2.5 SEM image of the grains of the reaction product AlNi.

In the DSC experiment of the cold rolled Ni/Al multilayer foil, three peaks can be identified in the constant-heating-rate DSC curve, as shown in Figure 2.6. A DSC curve for a PVD foil with the bilayer thickness of 70 nm is also shown in Figure 2.6 for comparison. There are also three peaks in this DSC curve. However, the shapes of the three peaks are different in the two DSC curves. Moreover, the peak temperatures for the cold rolled foil are much higher than those for the PVD foil. This is due to the much bigger bilayer thickness (several micrometers for the cold rolled foils versus tens of nanometers for the PVD foils) and the non-uniform structure of the cold rolled foils.

In the DSC curve for the cold rolled Ni/Al multilayer foil, peak A is much broader than peak B and C. It extends from 430°C to 630°C for the cold rolled foil. Previous numerical simulations and theoretical calculations suggested that a burst of nucleation occurring heterogeneously at boundaries in the interface plane rather than randomly over the whole interface area during formation process in reactive thin films can result in broad peaks in DSC curves [42, 43]. For the cold rolled Ni/Al multilayer foils with non-uniform interface area, the broad peak A in the DSC scan is due to the spatial bias (the deviation from spatial randomness) in the nucleation of product phase.

2.3.4 Reaction Process Analysis

To identify the evolution of reaction products at the different reaction stages for the cold rolled Ni/Al multilayer foils, some of the foils were preheated to 350 °C (the temperature slight below the onset temperature of peak A in the DSC curve), 530 °C (the midpoint temperature of peak A in the DSC curve), 640 °C (the midpoint temperature of peak B in the DSC curve) and 725 °C (the maximum temperature for the DSC scans) using the

same heating rate as in the previous DSC runs. Figure 2.7 shows the XRD pattern and SEM image for the cold rolled foil heated to 350 °C. They are similar to those for the as cold rolled foils. Only Ni and Al can be identified in the preheated foil. For the cold rolled foil heated to 530 °C and 640 °C (Figures 2.8 (a) and 2.8 (b)), Al_3Ni peaks appear among the Ni and Al peaks, suggesting that Al_3Ni was generated at these temperatures. For the foil annealed to 530 °C, Al_3Ni layers can be observed at isolated sites along the Ni/Al interface. The inset in Figure 2.8 (a) suggests that the peak A in the DSC curve is associated with the growth of Al_3Ni at isolated nucleation sites. In the foil annealed to 640 °C, the Al_3Ni layers are continuous, fully covering Ni particles. Also, growth in thickness towards the neighboring Ni particles can be observed (Figure 2.8 (b)). This suggests that peak B in the DSC curve is related to the growth of Al_3Ni in the direction normal to the Ni/Al interface. Therefore both DSC peaks A and B in the DSC curve of the cold rolled Ni/Al multilayer foils are associated with the exothermic formation of Al_3Ni. This is in agreement with Coffey's interpretation of the two exothermic DSC peaks that were observed for the formation of a single phase [40]. In Coffey's model, it was assumed that the generation of Al_3Ni occurred as a two-stage process. The first step was the lateral growth of Al_3Ni phase from isolated nucleation sites and the subsequent coalescence into a continuous layer. The second step was the growth of such Al_3Ni layers in the direction normal to the interface until all Al was consumed. Our XRD and SEM results support Coffey's model for the two-stage formation process of Al_3Ni. For the cold rolled foils heated to 725 °C (Figure 2.9), three phases can be identified: the final reaction product, AlNi, the intermediate reaction product Al_3Ni and the remaining unreacted Ni.

Thus the last peak (peak C) in the DSC scan is associated with the formation of the final product, AlNi.

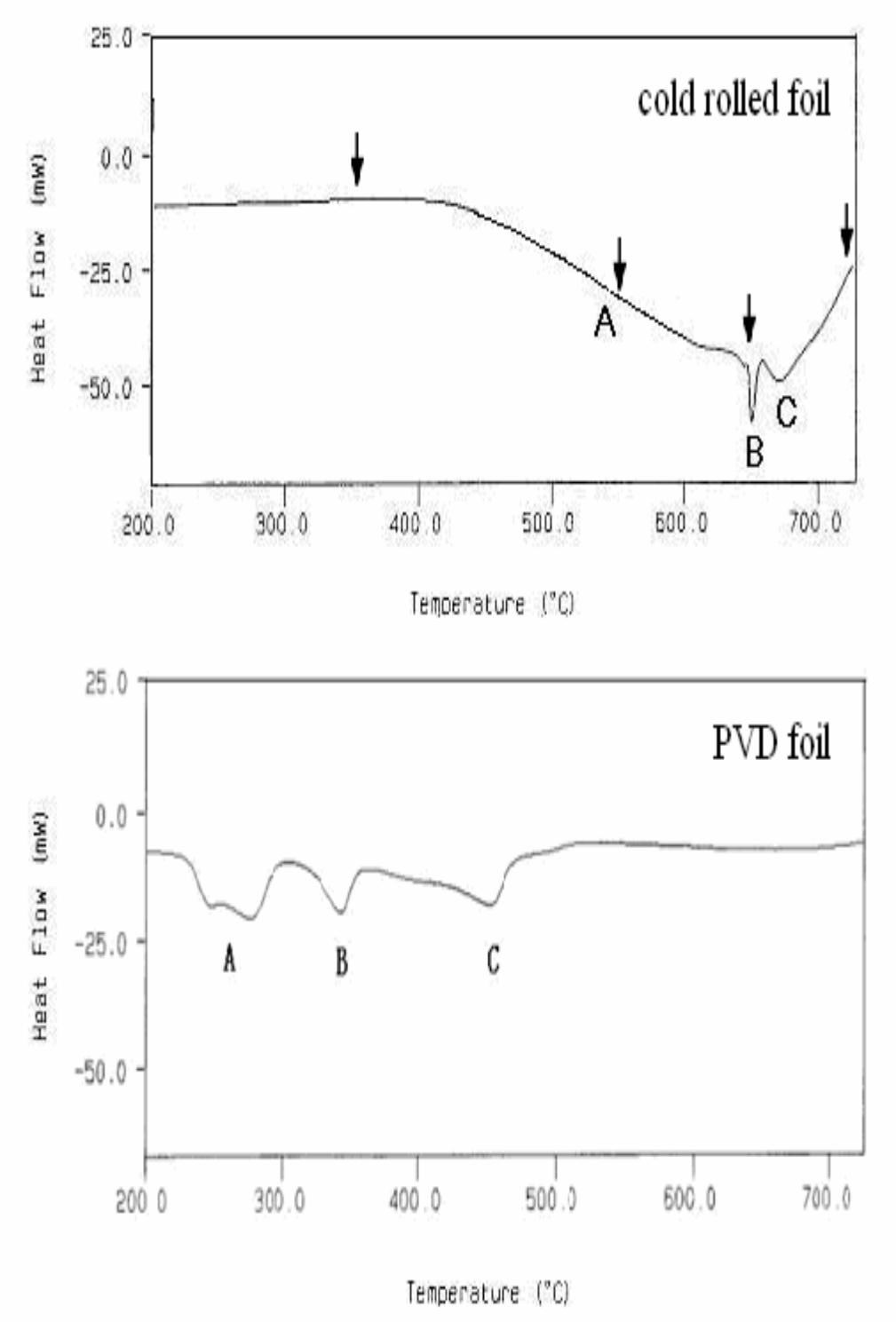

Figure 2.6 DSC curve for the as cold rolled and PVD Ni/Al multilayer foil.

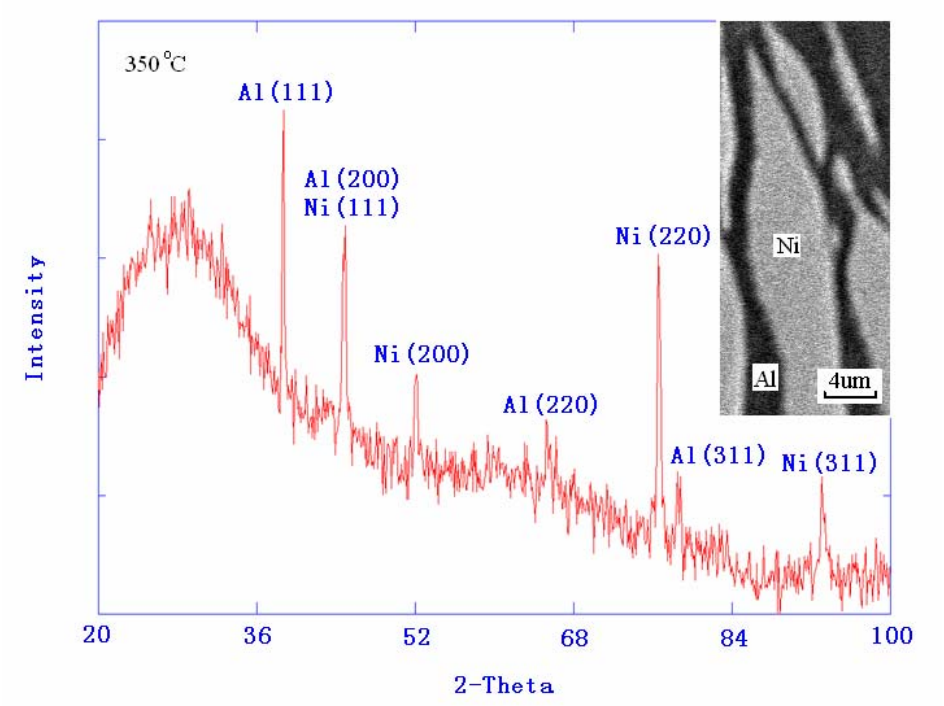

Figure 2.7 XRD pattern and SEM images for the as cold rolled Ni/Al multilayer foils heated to 350°C.

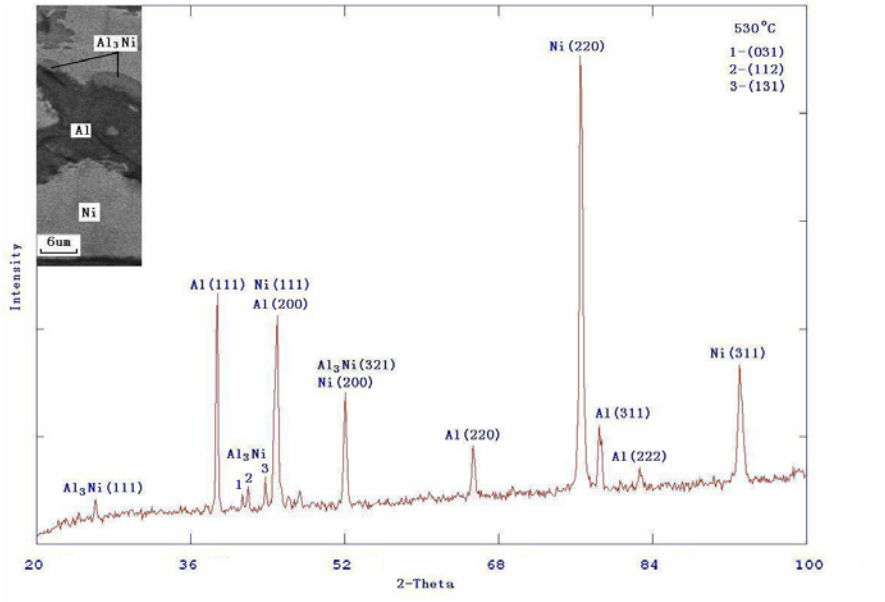

Figure 2.8 (a) XRD pattern and SEM images for the as cold rolled Ni/Al multilayer foils heated to 530°C.

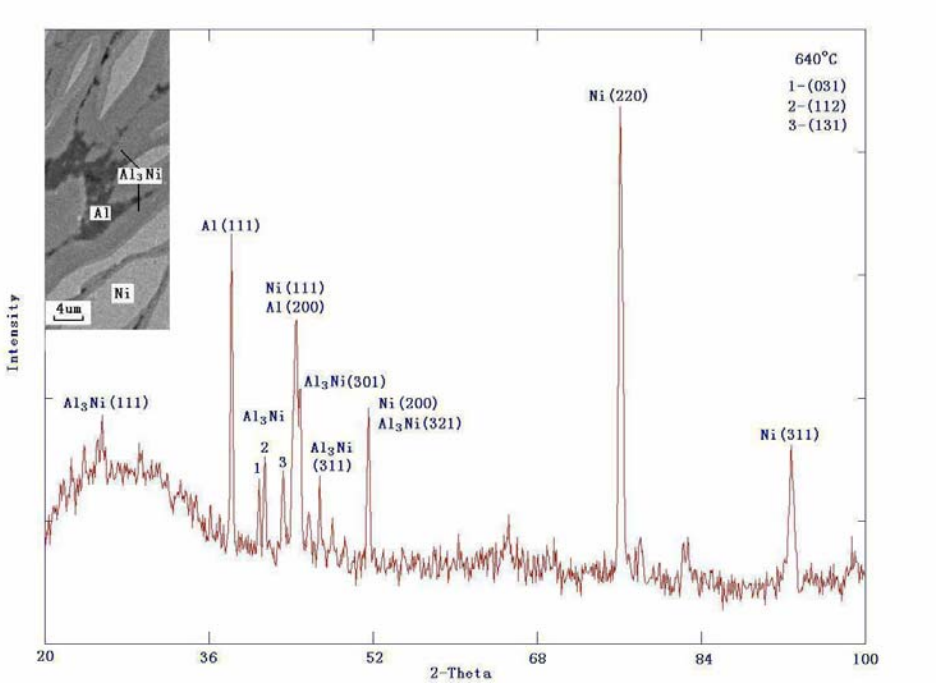

Figure 2.8 (b) XRD pattern and SEM images for the as cold rolled Ni/Al multilayer foils heated to 640°C.

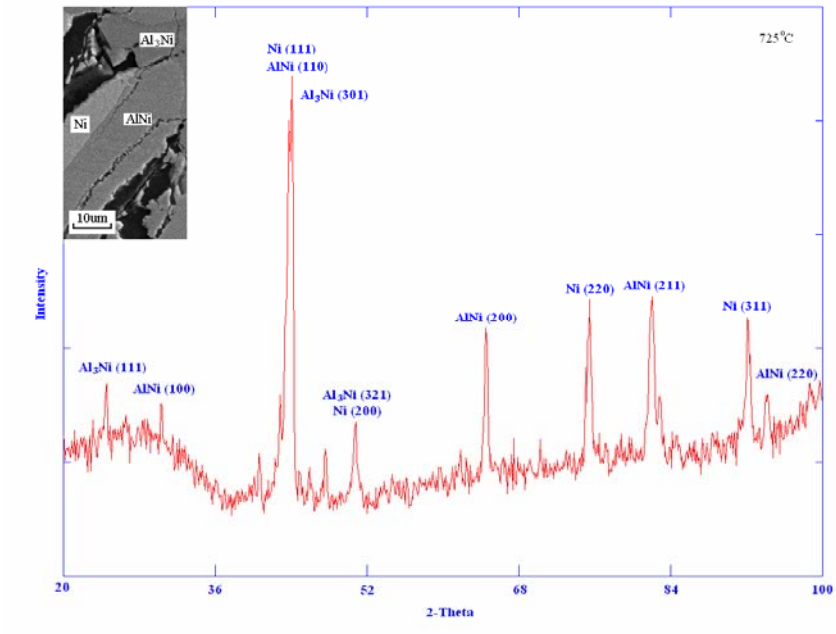

Figure 2.9 XRD pattern and SEM images for the as cold rolled Ni/Al multilayer foils heated to 725°C.

By integrating the net heat flow with respect to time in the DSC curves, the enthalpy of the reaction for the cold rolled foil and the PVD foil are calculated to be -57.5 kJ/mol and -57.9 kJ/mol, respectively. The calculated values are slightly smaller than the formation enthalpy of AlNi (-59 kJ/mol) [41]. For the cold rolled foil, this is due to the incomplete reaction of the foil. As was shown previously, unreacted Ni remained with Al_3Ni in the foil that was heated to the maximum temperature of 725 °C (Figure 2.9, the volume ratio of the remaining Ni in the foils can be estimated to be less than 8%, so the calculated heat of reaction is still in agreement with the literature value). Whereas, for the PVD foil, the slightly smaller heat of reaction might be due to prior intermixing that occurred during the deposition process.

2.4 Characterization of the Partially Reacted Ni/Al Multilayer Foils

In order to identify the two distinct reaction steps observed in the ignition experiment, some Ni/Al multilayer foils were quenched so that the first reaction step terminated in the middle of the foils.

2.4.1 SEM Experiment

Figure 2.10 shows the SEM images of a quenched Ni/Al multilayer foil. At one end of the foil, necked Ni particles were embedded in the Al matrix, showing that no reaction occurred (Figure 2.10 (a)). At the middle of the foil, where the reaction was quenched, a thin layer of Al rich phase (the Ni/Al atomic ratio obtained by EDX is approximately 1/3) can be seen to grow around the necked Ni particles. Such Al rich layers were distributed at isolated sites and did not fully cover the Ni particles (Figure 2.10 (b)). Figure 2.10 (c) shows the part of Ni/Al foil that completed the first reaction step, where the Al rich layers

continued to grow and fully encircled the Ni particles. In this study, this kind of foil is defined as partially reacted foil. In Figure 2.10 (d), these Al rich layers began to grow in thickness and spread to the neighboring Ni particles. According to Coffey's model and the microstructures at various positions of the quenched foil, figure 2.10 (b) and figure 2.10 (c) show the parts of the foil that experienced the growth of the Al rich phase from isolated nucleation sites and the subsequent coalescence into a continuous layer, which represent the first formation stage of the Al rich phase. Figure 2.10 (d) shows the growth of the Al rich layers in the direction perpendicular to the interface, which represents the second formation stage of the Al rich phase. So this two step reaction process provides a direction experimental evidence for Coffey's model in the self-propagating reaction of reactive multilayer foils.

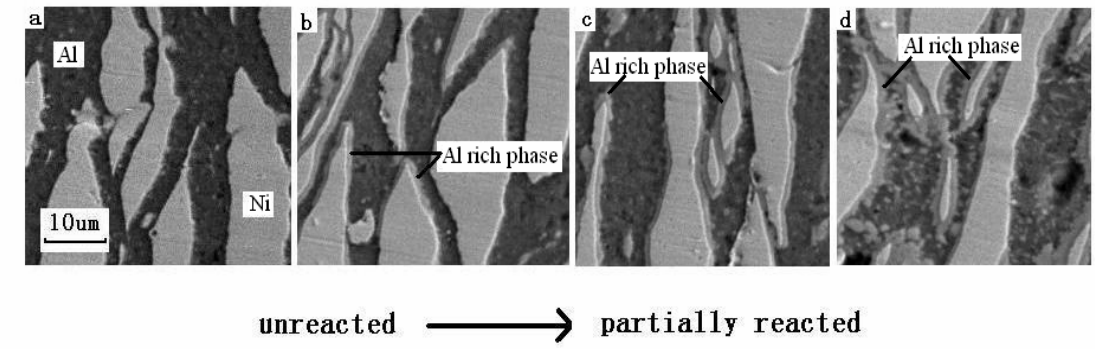

Figure 2.10 SEM images of a quenched Ni/Al multilayer foil.

2.4.2 DSC Experiment

DSC curve for the partially reacted foil are shown in Figure 2.11. There are also three exothermic peaks in the DSC scan. However, there are some differences between the DSC curves of the as cold rolled foil and the partially reacted foil. Peak A of the partially reacted foils (onset starts at about 500 °C) is much smaller than the as cold rolled foils

(onset starts at about 430 °C), which suggests that the first stage of reaction has already occurred in the partially reacted foils. Additionally, the three peak temperatures for the partially reacted foils are higher compared with the as cold rolled foils, indicating that more energy input from DSC is needed to complete the same phase formation process. These high peak temperatures are due to the occurrence of the first stage of reaction prior to the DSC experiment in the partially reacted foils. So less energy can be released from the foils during the DSC experiment.

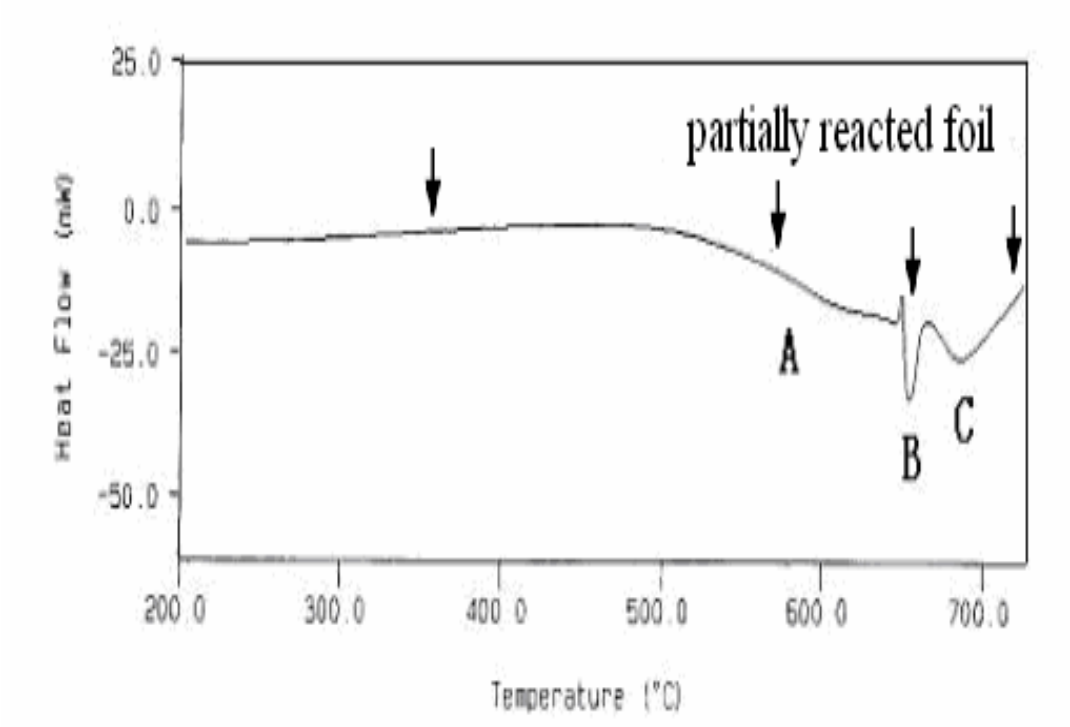

Figure 2.11 DSC curve for the partially reacted Ni/Al multilayer foil.

2.4.3 Reaction Process Analysis

To identify the reaction products for the different reaction stages, some of the partially reacted foils were heated to 350 °C (below the onset temperature of peak A in the DSC curve), 550 °C (the midpoint temperature of peak A in the DSC curve), 660 °C (the

midpoint temperature of peak B in the DSC curve) and 725 °C (the maximum temperature for the DSC scans) using the same heating rate as in the previous DSC runs. Figure 2.12 shows the XRD patterns and SEM image for the partially reacted foil heated to 350 °C. Unlike the cold rolled foil annealed to 350 °C which only contains Ni and Al (Figure 2.7), Al_3Ni layers (the Ni/Al atomic ratio obtained by EDX is approximately 1 to 3) can be observed at isolated sites at the Ni/Al interface. This confirms that the first stage of reaction observed in the ignition experiments is associated with the growth of Al_3Ni at isolated nucleation sites at the Ni/Al interface. For the partially reacted foils heated to 550 °C and 660 °C, the XRD traces and SEM images are similar to the cold rolled foils that were heated to 530 °C and 640 °C. For the partially reacted foil heated to 550 °C, Al_3Ni layers appear at isolated sites along the Ni/Al interface (Figure 2.13 (a)), and for the partially reacted foil heated to 660 °C, the Al_3Ni layers are continuous, cover the whole Ni particles, and grow in thickness towards the neighboring Ni particles (Figure 2.13 (b)). Thus both the first two peaks (A and B) in the DSC curve of the partially reacted Ni/Al multilayer foils could be identified as the exothermic formation of Al_3Ni. The XRD and SEM results of the partially reacted foils give another experimental proof for Coffey's model for the two-stage formation process of Al_3Ni. For the partially reacted foils heated to 725 °C (Figure 2.14), there are also three phases in the foil: the reaction product, AlNi, Al_3Ni and the remaining unreacted Ni. Thus the last peak (peak C) in the DSC scan for the partially reacted foils is also associated with the formation of the final product, AlNi.

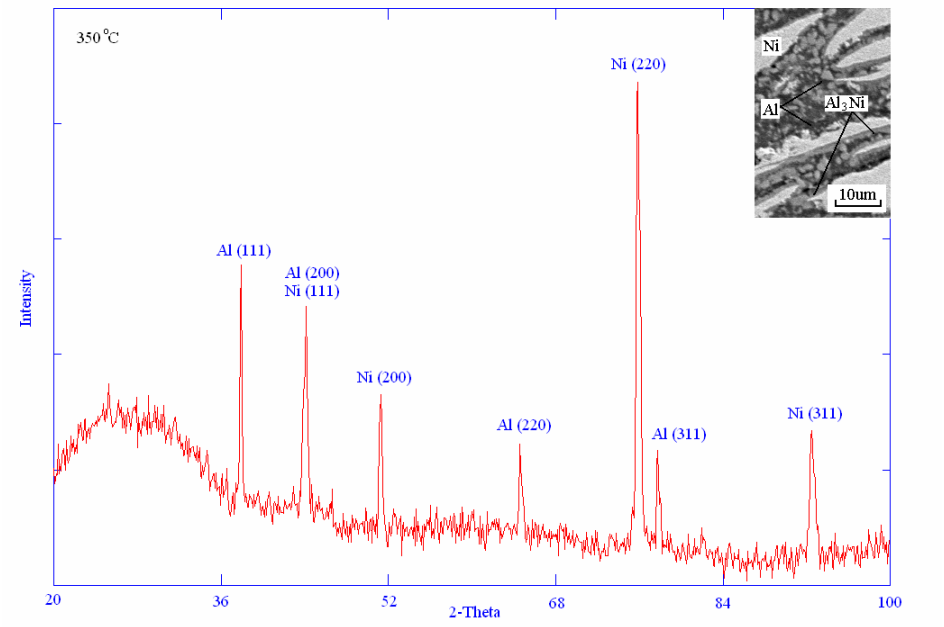

Figure 2.12 XRD pattern and SEM images for the partially reacted Ni/Al multilayer foils heated to 350°C.

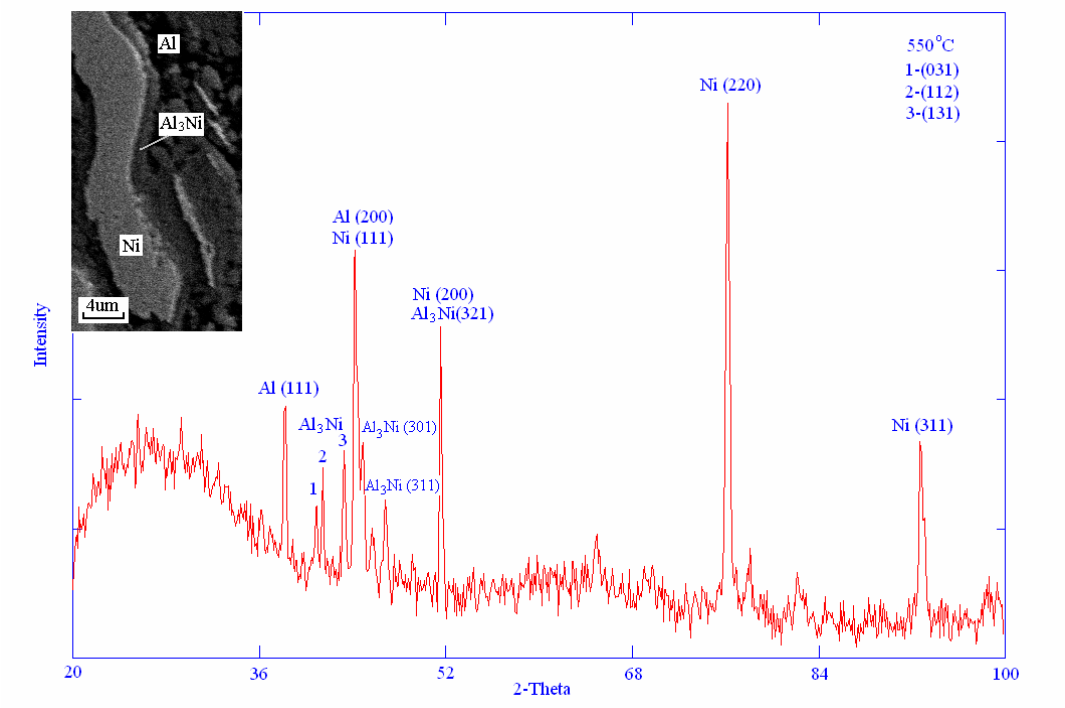

Figure 2.13 (a) XRD pattern and SEM images for the partially reacted Ni/Al multilayer foils heated to 550°C.

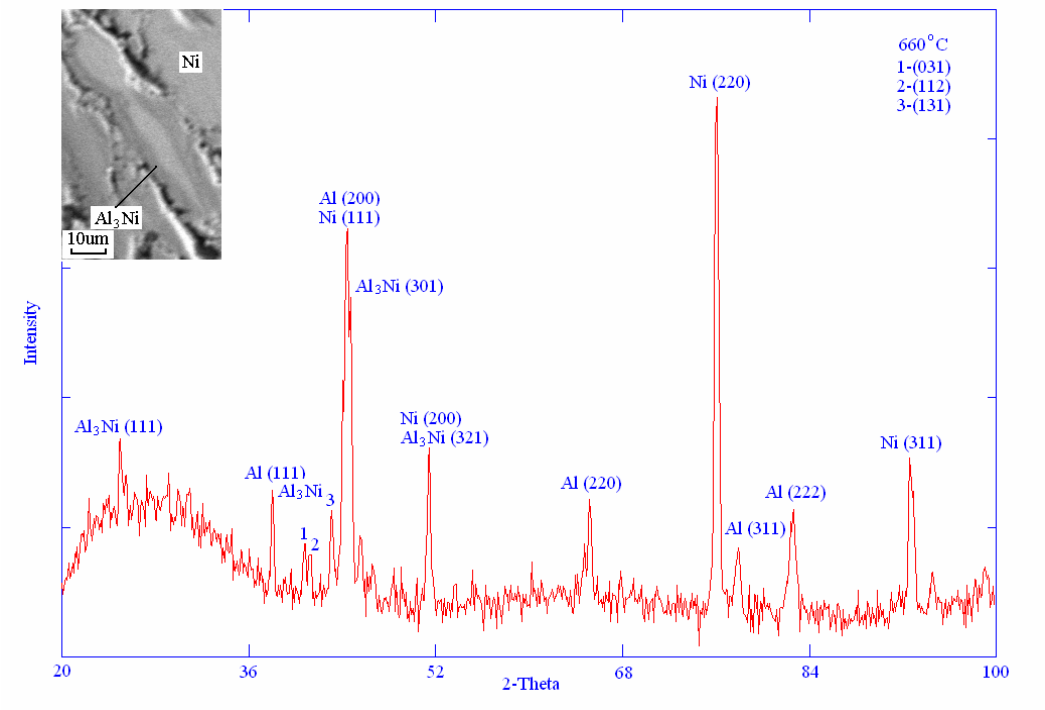

Figure 2.13 (b) XRD pattern and SEM images for the partially reacted Ni/Al multilayer foils heated to 660°C.

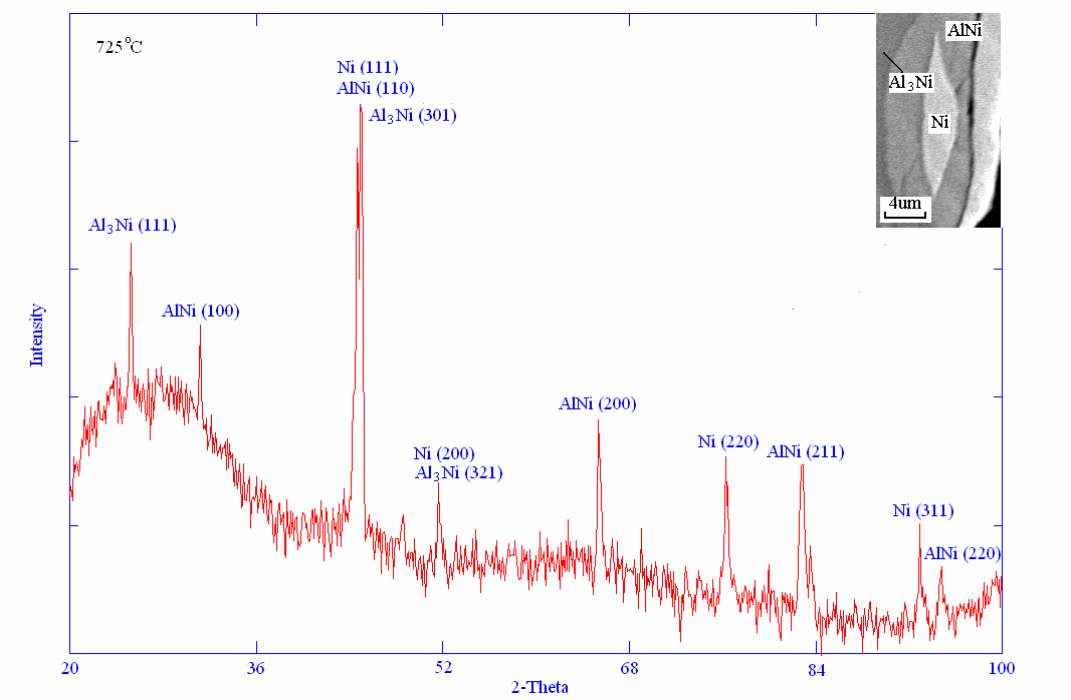

Figure 2.14 XRD pattern and SEM images for the partially reacted Ni/Al multilayer foils heated to 725°C.

2.5 Reaction Process for the Cold Rolled Ni/Al Multilayer Foils

According to the DSC curves, SEM observation, and XRD scans of both the as cold rolled and the partially reacted Ni/Al multilayer foils at various formation stages, the entire reaction process for the cold rolled Ni/Al multilayer foils can be identified. The first reaction stage with slow reaction front propagation was the lateral growth of Al_3Ni phase from isolated nucleation sites and the subsequent coalescence into a continuous layer. This stage was associated with the broad peak A in the DSC curve and defined as stage one of the formation process of Al_3Ni. The next reaction stage with fast reaction front propagation was the growth of the Al_3Ni layers in the direction normal to the interface until all Al was consumed. This stage was related to peak B in the DSC curve and defined as stage two of the formation process of Al_3Ni. Afterwards, Al_3Ni reacted with the remaining Ni to form the final reaction product, AlNi, corresponding to peak C in the DSC scan. The entire formation process is schematically illustrated in Figure 2.15.

2.6 Reaction Velocities for the Cold Rolled Ni/Al Multilayer Foils

The reaction velocities of the cold rolled foils were measured by a digital camcorder, with a temporal resolution of 0.03 seconds. The measured speed was around 7mm/s, which was much smaller than the reaction speed in the Ni/Al multilayer foils made by PVD methods with reaction velocities ranging between 1-30 m/s. The lower speed in the cold rolled foils was due to the much larger Ni/Al bilayer thickness, which was estimated to be in the range of several micrometers. As the bilayer thickness becomes larger, the atomic diffusion distances are bigger, and, therefore, atoms mix more slowly. So that heat is released at a lower rate and the reactions travel more slowly through the foil. In addition, the alternating Ni/Al layers in the cold rolled foil were not uniform, thus making

it difficult to ignite the foil and reducing the speed of the self-propagating reaction. In spite of such shortcomings of cold rolled multilayer foils, this method has its own advantages such as the ease of fabrication, low-cost and less time consuming nature. Meanwhile, the reduction in reaction velocity also made the cold rolled foil an ideal sample to study the details of the formation reactions in multilayer foils.

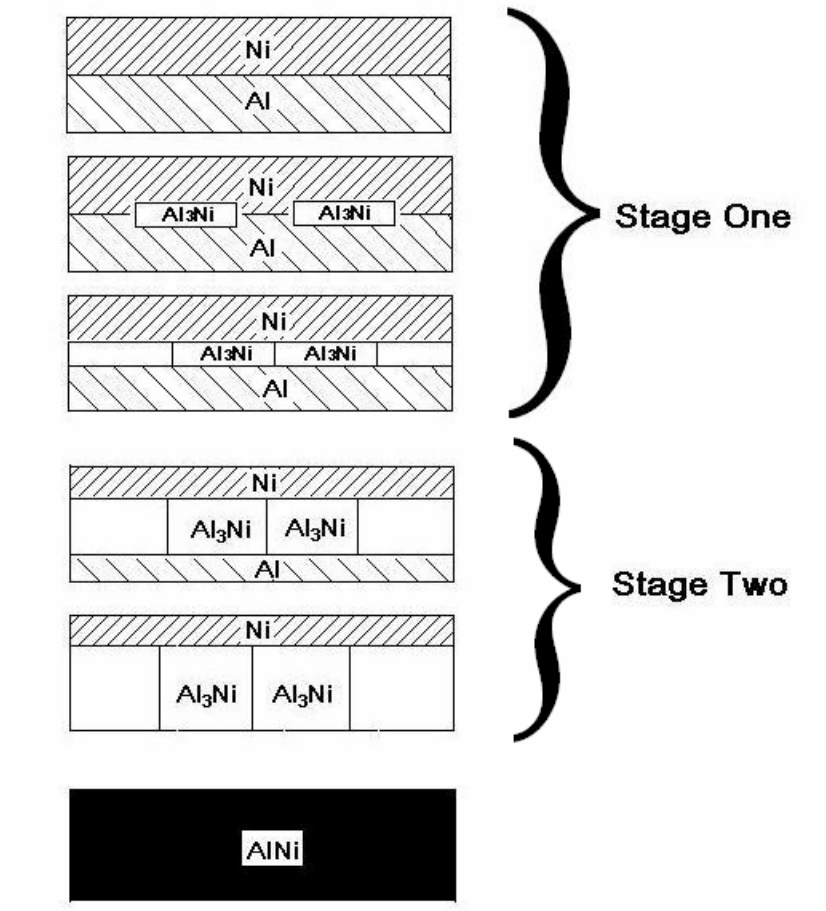

Figure 2.15 Schematic illustration of the formation process of Al_3Ni and AlNi.

3. EXOTHERMIC REACTIONS IN COLD ROLLED TI/AL REACTIVE MULTILAYER FOILS

Exothermic reactions of Ti and Al leading to the formation of metastable titanium aluminide phases have been the subject of considerable study. Numerous experiments using techniques such as X-ray diffraction, electron diffraction, light optical microscopy, differential scanning calorimetry, and Rutherford back scattering spectrometry have shown that the trialuminide phase, Al_3Ti, forms first in both bulk (Ti and Ti/Al alloys coated with a pure solid Al layer) [46] and thin-film samples of Ti/Al [47].

In this study, Ti/Al multilayer foils were also fabricated by cold rolling to test whether this method can be extended to fabricate other metal/aluminum multilayer systems.

3.1 Fabrication of Ti/Al Multilayer Foils by Cold Rolling

Ti/Al multilayer foils were fabricated by a cold rolling method similar to the method for the Ni/Al multilayer foils mentioned in chapter 2.

Thin sheets (3 inch by 3 inch square) of pure elements of Ti and Al with initial thickness of 32 μm and 38.1μm respectively (Alfa Aesar Company, Ti minimum purity of 99.6%wt and McMaster Company, Al minimum purity of 99%wt) were alternatively stacked together in order to obtain a 1/1 atomic ratio of Ti/Al. The stacked sheets were placed in between a folded stainless steel sheet, which was previously hardened by repeated rolling. This assembly was cold rolled a few times using a laboratory rolling mill to reduce the thickness to half of the original thickness. Afterwards the Ti/Al sheets were taken out of the stainless steel sheet, cut into halves, stacked the halves together to recover their original thickness, and then cold rolled without changing the distance between the rollers

(this is defined as a rolling cycle). After several rolling cycles, a uniform Ti/Al multilayer foil was achieved. The total thickness of the foil was around 280 μm. As Ti is much harder than Ni, it is more difficult to make homogeneous Ti/Al multilayer foils and the resulting foils fall apart easily.

3.2 Ignition of the Cold Rolled Ti/Al Multilayer Foils

The cold rolled Ti/Al multilayer foils were ignited by a flame. After heating for several seconds, an exothermic reaction occurred in the foil. But different from the Ni/Al foils, the reaction in Ti/Al foils was not self-propagating. Only the parts of the foil which were put in the flame reacted, indicating more heat was needed to trigger the reaction. And if the foil was taken out of the flame, the reaction would stop, suggesting it can not produce enough heat to sustain the reaction.

There was also a two-step reaction observed in the Ti/Al foils. At the step one, the reaction spread along the direction parallel to the surface of the foil and the foil surface became darker. Then at step two, the reaction released a large amount of heat and showed visible red light. Both of these two reaction steps have a low reaction velocity.

3.3 Characterization of the Cold Rolled Ti/Al Multilayer Foils

Figure 3.1 shows the XRD pattern and SEM image of the as cold rolled Ti/Al multilayer foils. In the XRD trace of the as cold rolled Ti/Al foils, all the peaks correspond to Al and Ti. In the SEM image, no sign of reaction can be observed in the as cold rolled Ti/Al multilayer foil. Necked Ti particles are embedded in the Al matrix and aligned along the rolling direction. Most of the Ti particles possess a wavy surface. There are also some cracks between the necked Ti particles and the Al matrix. This is because Ti is a hard

material and it is difficult to deform Ti. The presence of the cracks can also explain why the cold rolled Ti/Al foils fall apart easily and why it needs more heat from the flame to sustain the reaction. The interface area between Ti and Al is reduced due to the presence of the cracks resulting in less interface reaction and less heat released from the foil itself.

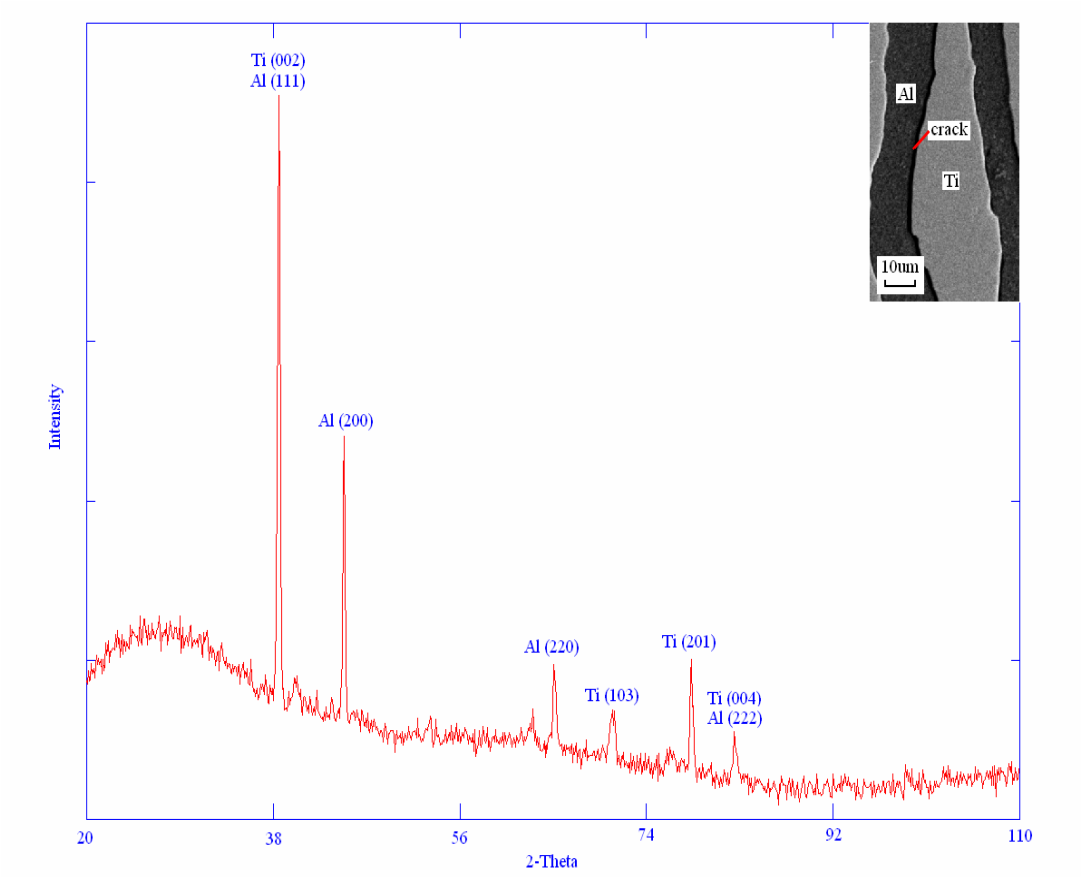

Figure 3.1 XRD pattern and SEM image of an as cold rolled Ti/Al multilayer foil.

Figure 3.2 shows the XRD pattern and SEM image of the final reaction product of the Ti/Al multilayer foils. Two phases can be observed in the reacted foil: AlTi as the reaction product and some remaining Ti. Some Al_3Ti may also exist since the atomic ratio of Al/Ti in the foil is a little higher than 1/1. There are also many pores in the

reacted foil, which result from the contraction during rapid cooling and the density increase during the reaction.

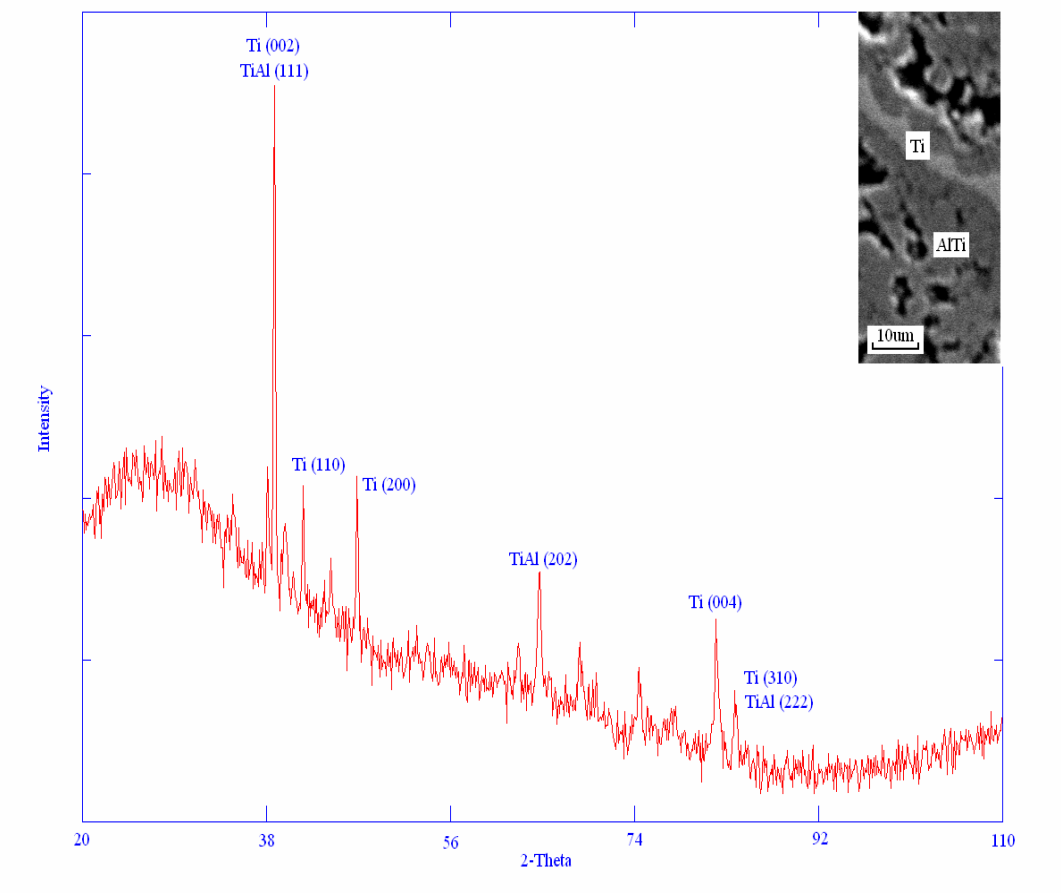

Figure 3.2 XRD pattern and SEM image of the reaction product of Ti/Al multilayer foils.

In order to identify the two distinct reaction steps observed in the ignition experiment, some Ti/Al multilayer foils were quenched after they finished the first reaction step. These kinds of foils are defined as partially reacted foils.

Figure 3.3 shows the XRD pattern and SEM image of such partially reacted Ti/Al multilayer foils. Besides Ti and Al, Al_3Ti layers (the Ti/Al atomic ratio obtained by EDX is approximately 1 to 3) can be observed at isolated sites at the Ti/Al interface. This

suggests that the first step of reaction observed in the ignition experiments is associated with the growth of Al_3Ti at isolated nucleation sites at the Ti/Al interface.

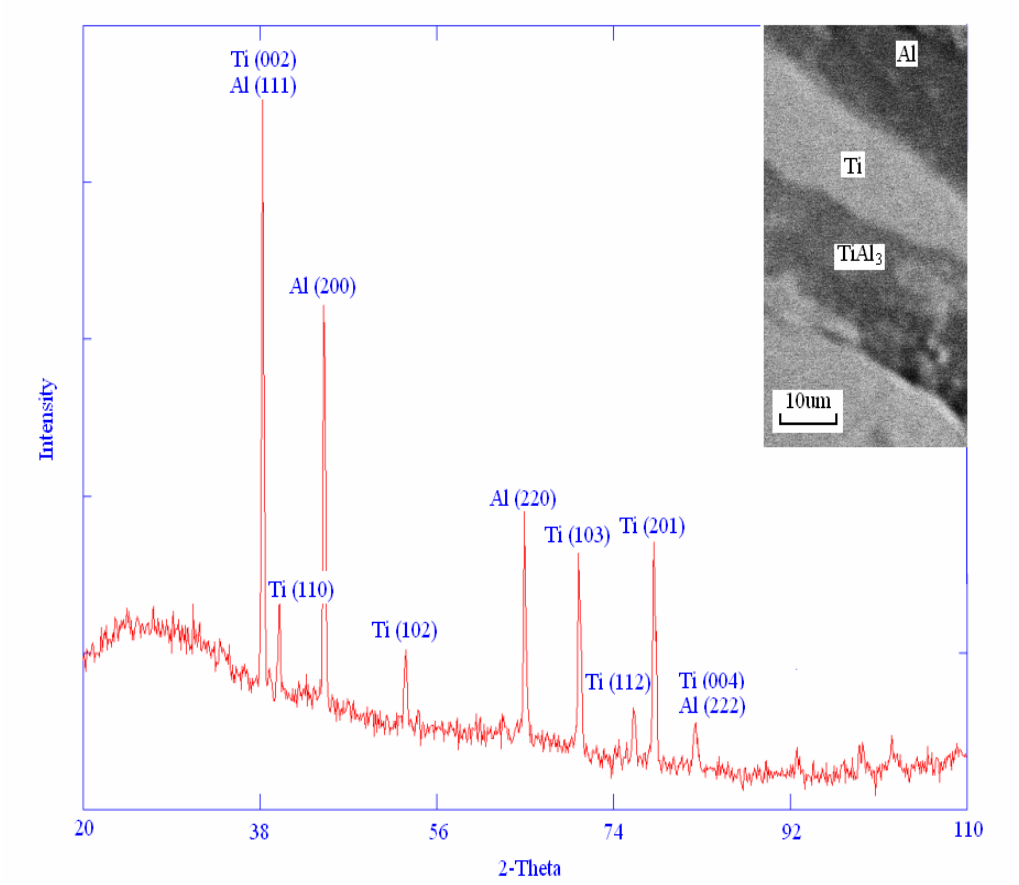

Figure 3.3 XRD pattern and SEM image of a partially reacted Ti/Al multilayer foil.

3.4 Reaction Process for the Cold Rolled Ti/Al Multilayer Foils

According to the SEM and XRD results of the as cold rolled, the partially reacted Ti/Al multilayer foils and their final reaction products, the entire reaction process for the cold rolled Ti/Al multilayer foils can be identified, which is assumed to be similar to the cold rolled Ni/Al multilayer foils. The first reaction stage was the lateral growth of Al_3Ti phase from isolated nucleation sites and the subsequent coalescence into a continuous layer. The next reaction stage was the growth of the Al_3Ti layers in the direction normal

to the interface until all Al was consumed. Afterwards, Al_3Ti reacted with the remaining Ti to form the final reaction product, AlTi. Further DSC experiments are required to confirm this assumption for the reaction process of the cold rolled Ti/Al multilayer foils.

From the fabrication of cold rolled Ni/Al and Ti/Al multilayer foils, it is clear that the cold rolling method can be used as a general fabricating method to make metal/Al reactive multilayer foils and can be potentially extended to fabricate other reactive multilayer systems.

3.5 Cold Rolled Foils vs. PVD Foils

As mentioned in chapter 2, in the cold rolled reactive multilayer foils, the bilayer thickness was estimated to be in the range of several micrometers. As the bilayer thickness becomes larger, the atomic diffusion distances are bigger, and, therefore, atoms mix more slowly. So that heat is released at a lower rate and the reactions travel more slowly through the foil. In addition, the alternating layers in the cold rolled foil were not uniform, thus making it difficult to ignite the foil and reducing the speed of the self-propagating reaction. So these kinds of cold rolled Ni/Al and Ti/Al reactive foils are not suitable local heat sources to be used in joining applications. Further development is required to refine this cold rolling method to fabricate reactive foils which possess the alternating layers with similar thickness as the PVD foils. In the following chapters, PVD foils were used to conduct the silicon wafer bonding experiments and the simulation of the reactive foil joining process.

4. NUMERICAL SIMULATION OF REACTIVE FOILS JOINING PROCESS

One of the major applications of the reactive multilayer foils is that they can be used as local heat sources to melt solder or braze layers and thereby join different components. A lot of materials have been reported to be joined successfully by reactive multilayer foils, such as stainless steel, aluminum, titanium, metallic glass, silicon, and MEMS (Microelectromechanical Systems) elements [23, 26, 28, 30, 32, 53].

The major advantages in reactive foil joining are as follow. Reactive foil joining does not need furnaces or other external heat sources because exothermic reaction in reactive foil can be carried out at room temperature in air; thermal damage is very small in joining temperature-sensitive materials or components because of very localized heating at the interface between materials during reactive jointing; reactive foils can join materials with different coefficients of thermal expansion, such as metals and ceramics. The rapid nature of the process reduces oxidation of the molten solder or braze and very limited heating of the components dramatically reduces thermal stress in the components being joined.

Wang *et al.* developed a numerical method to predict the amount of AuSn solder layer that melted as the reactive foil thickness was varied and to simulate the evolution of temperature profiles within the bonded components [23]. In this study, a new numerical simulation of the reactive joining process was conducted using a commercial software Fluent to predict the temperature distribution in the bonding components. The simulation was first performed on joining of stainless steel components. Then, the simulation was also conducted to predict the temperature evolution during the reactive joining process of silicon wafers.

4.1 Numerical Model

The commercial CFD software, Fluent, was used to simulate the two-dimensional heat transfer in the joining geometry and to predict the temperature evolution in the joined components during the joining process. Figure 4.1 shows the geometry of the reactive joining process. Since it is a symmetric structure, we can take one half of this geometry to conduct the simulation, which is shown in Figure 4.2. All the dimensional parameters of different parts in the joining geometry are listed in Table 4.1.

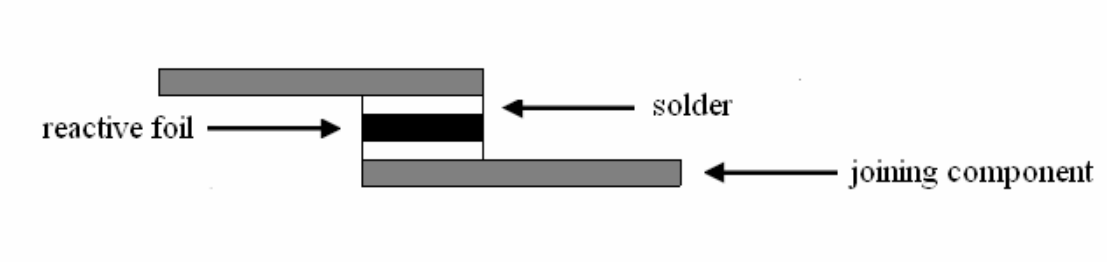

Figure 4.1 The geometry of the reactive joining process.

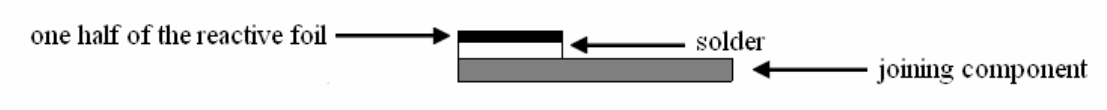

Figure 4.2 The geometry of the simulation.

Table 4.1 Dimensional parameters of different parts in the joining geometry.

	Length (mm)	Width (mm)	Thickness (μm)
Stainless steel	25.4	6.35	500
Reactive foil	12.7	6.35	70
Solder	5	6.35	25

The governing equation used in this model is the two-dimensional heat conduction equation:

$$k\frac{\partial^2 T}{\partial x^2}+k\frac{\partial^2 T}{\partial y^2}=\rho C_p\frac{\partial T}{\partial t} \tag{2}$$

In the equation above, k is thermal conductivity, ρ is density, and C_p is specific heat. The boundary conditions used in the modeling geometry are shown in Figure 4.3.

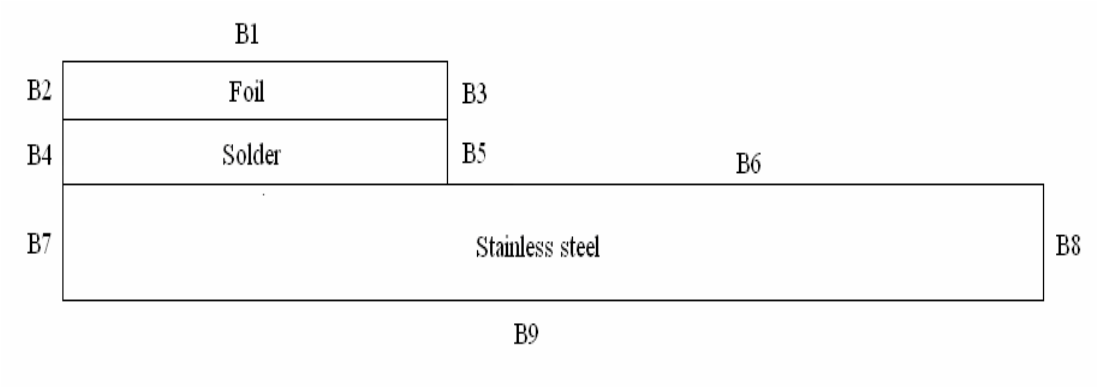

Figure 4.3 Boundary conditions used in the simulation.

Boundary condition 1:

$$k_f\frac{\partial T}{\partial x}=q \tag{3}$$

In the equation above, k_f is the thermal conductivity of the reactive foil, q is the heat flux during the reaction, which can be calculated using the formation enthalpy of AlNi (59 kJ/mol) and the reaction time.

Boundary conditions 2-9 are convection with a convection coefficient of 35 W/m^2K [55] and ambient air temperature of 293k.

Several thermophysical parameters for the reactive foil, solder, and stainless steel are listed in Table 4.2, which are used as input for the simulation.

Table 4.2 Thermophysical parameters for the reactive foil, solder, and stainless steel used in the simulation.

	Stainless steel	Solder	Foil (reacted)	Foil (unreacted)
Thermal conductivity (W/mK)	16.2	57	25	160
Heat capacity (J/kgK)	500	170	610	830
Density (g/cm^3)	7.99	14.51	5.86	5.55

The melting temperature for the AuSn solder is 280 °C, and the heat of fusion of the AuSn solder is 6.188 kJ/mol.

Work of Swiston *et al.* indicated that the reaction front in the reactive multilayer foils is essentially one-dimensional; although the reaction front propagates radially from the initiation point, the curvature of the reaction front is small relative to the thickness of the foil [52]. Thus we can treat the three-dimensional heat flow within the context of a two-dimensional model assuming linear motion of the reaction front. The computations focused on simulating thermal conduction of heat into and the temperature evolution within the joined components.

The thermal transport across the unbonded interfaces is considered using a thermal interface model, which accounts for thermal resistance at the interface between unbonded layers and assumes that the thermal resistance decreases exponentially when wetting occurs at the interface. The thermal conductance, h, which scales as the inverse of the contact resistance, is used to represent the effect of imperfections in contact between layers. As long as the temperature at the interface is below the melting temperature of the solder, the model assumes that $h \approx 2\times10^{3} W/m^{2}K$ (at room temperature, this value is obtained from Contact Conductance Estimator which is a database containing many empirical, lab-tested, credible data of different configurations of contact, collected from the engineering literatures) [54] and it increases exponentially with temperature, becoming infinite at the melting temperature of the solder corresponding to perfect thermal contact between the layers.

In this model, Ni/Al multilayer foils with bilayer thickness of 40 nm and AuSn solider ribbon (25 μm thick) were used. According to Gavens *et al.* [45], for the Ni/Al multilayer foils with bilayer thickness of 40 nm, the reaction velocity is around 6 m/s. So the total reaction time of the reactive foil with length of 5 mm in the joining process is 0.83 ms.

As mentioned before, after the reactive foil was ignited, a thin reaction zone propagated along the unreacted foil. So the foil before and after the reaction zone will have different thermophysical properties. In this model, we divide the reactive foil into several parts and change the thermophysical properties of different parts as the reaction front passes each part to take this effect into consideration.

The reactive foil was divided into 1 part, 5 parts, and 8 parts. The resulting interface (solder-stainless steel interface) temperature at the end of the reaction was calculated for these three cases. The results are listed in Table 4.3.

Table 4.3 Solder-stainless steel interface temperature at the end of the reaction with reactive foil divided into different parts.

Foil divided into different parts	Interface temperature (K)
1	687.7
5	678.5
8	680.0

From the table above, for the cases that the foil was divided into 1 and 5 parts, the interface temperature difference is 1.3%, while for the cases that the foil was divided into 5 and 8 parts, the interface temperature difference is only 0.2%. Therefore, if we divide the foil into 5 parts to do the simulation, the results will be acceptable. Although by dividing the foil into large number of parts the simulation will be much closer to the real reaction process, this will also introduce a large amount of calculation work. Thus for this study we divide the foil into 5 parts to conduct our computation of the temperature distribution during the reactive joining process.

Figure 4.4 shows the schematic structure of the simulation geometry for the reactive joining process. There are five parts of the foil and two thermal contact resistant layers, one between the foil and the solder, and the other between the solder and the stainless steel.

Within one part of the foil, 2000 grids were used to conduct the simulation (same grids were used in every layer with the dimension of one grid 5×10^{-6} m by 2.5×10^{-6} m). The reaction was initiated at part 1 of the foil, propagated through the foil, and ended at part 5. Thermophysical properties of the foil in different part vary accordingly. Two positions A (100 μm under the solder/stainless steel interface in the middle of the joining area) and B (100 μm away from the joining area on stainless steel surface) were selected to monitor the temperature distribution in the joining components during the reactive joining process.

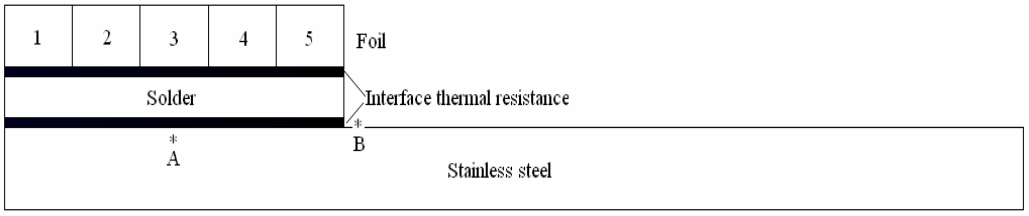

Figure 4.4 Schematic structure of the simulation geometry for the reactive joining process.

4.2 Simulation Results

From the joining geometry above, during the joining process the cooling time for the entire stainless steel specimen to decrease to 40 °C is calculated to be 100 s. In order to speed up the cooling process, the joining process can be performed between two stainless steel substrates. Table 4.4 shows the cooling time for the temperature of the whole piece of stainless steel specimen to decrease to 40 °C with different thicknesses of substrates.

From the calculation results, it can be concluded that a much more rapid cooling can be achieved by putting the joining components between two thick stainless steel substrates.

Table 4.4 Cooling time for the whole piece of stainless steel specimen with different thicknesses of substrates.

	Cooling time (s)
Stainless steel with no substrates	100
Stainless steel with 1 mm thick substrates	80
Stainless steel with 1 cm thick substrates	5

Figure 4.5 and 4.6 show the temperature evolution within 200 ms at position A and B with a foil thickness of 70 μm and two 1 cm thick stainless steel substrates. The two plots show that the highest temperature at position A and B are 231 °C and 119 °C, respectively; the temperature decreases to 91 °C for position A and 67 °C for position B after 200 ms. These results indicate that the heating area during the reactive joining process is highly localized, with very limited thermal exposure to the joining components.

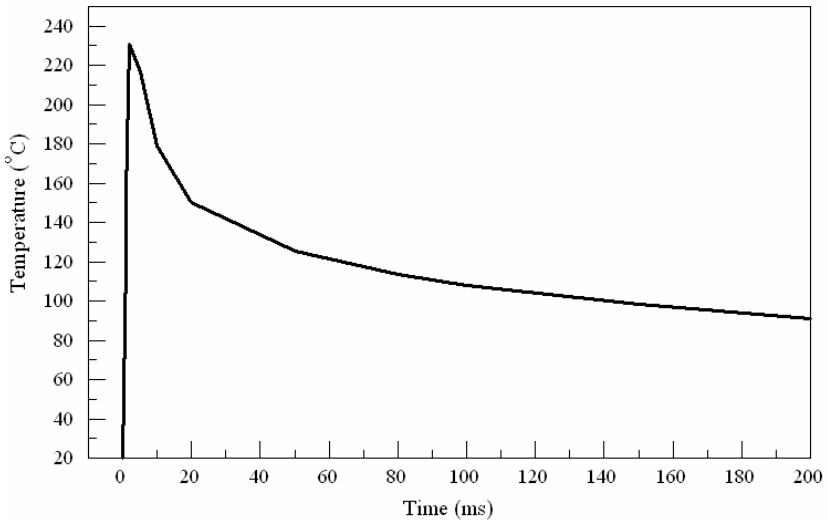

Figure 4.5 Temperature evolutions within 200 ms at position A with a foil thickness of 70 μm and two 1 cm thick stainless steel substrates.

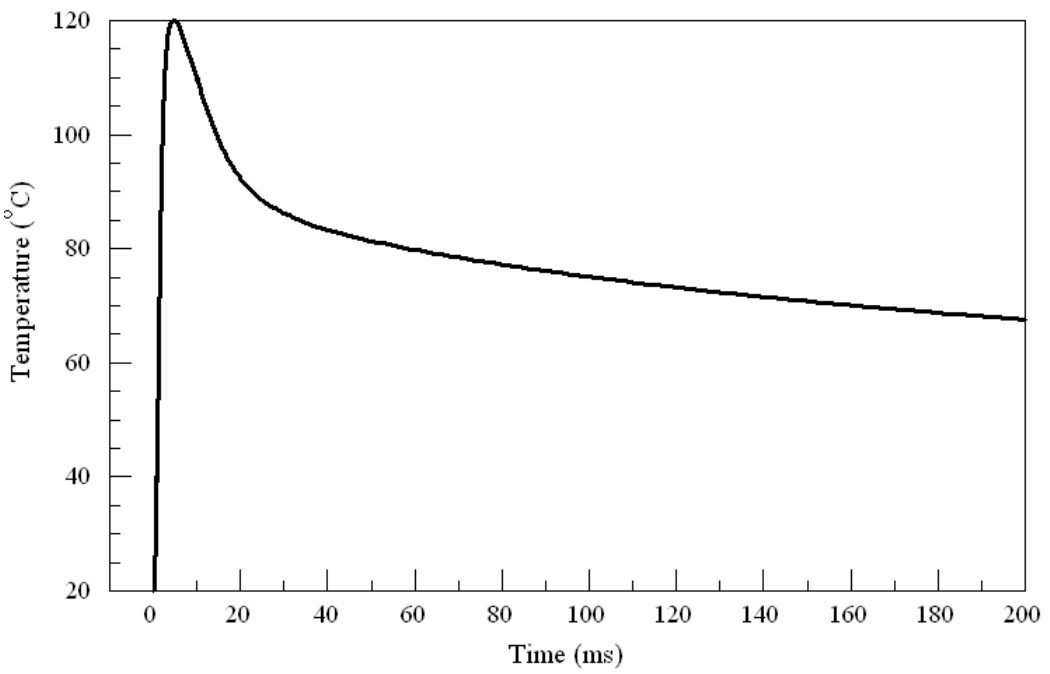

Figure 4.6 Temperature evolutions within 200 ms at position B with a foil thickness of 70 μm and two 1 cm thick stainless steel substrates.

These results also indicate that besides localized heating, a rapid cooling is achieved by this joining method. The localized heating and the rapid cooling are the major advantages of joining using the reactive multilayer foils. This simulation outcome is in agreement with the results of Wang *et al* [23].

5. REACTIVE MULTILAYER FOILS FOR SILICON WAFER BONDING

Various bonding methods have been reported for silicon wafer bonding applications, such as anodic bonding, direct bonding, and intermediate layer bonding including glass-frit bonding, thermocompression bonding, eutectic bonding, solder bonding, and adhesive bonding [56-59].

Anodic bonding (or electrostatic bonding) is commonly used in bonding silicon wafers. Anodic bonding technology was first introduced by Wallis and Pomerantz [60]. In their studies, polished glass and metal parts were assembled and heated in air to a temperature well below the softening point of the glass. A DC power supply is connected to the glass-metal assembly so that the metal is positive with respect to the glass. When a voltage in excess of several hundred volts is applied for several minutes, the glass and the metal formed a strong seal. The anodic bonding technique has been further developed for Si to glass, Si to Si, and Si to thin film wafer bonding at moderate temperature (300 °C – 450 °C) by applying a high DC voltage to the wafer pair (500 – 1000 V). The advantage of anodic bonding is that two dissimilar materials can be bonded together to form a strong and hermetic seal with little change in component dimensions. However, the bonding surfaces have to be polished and thoroughly cleaned to achieve strong bonding. Another disadvantage of anodic bonding is that the electrical field and high temperature are likely to affect the electrical properties and performance of the bonded structures.

Direct bonding (or fusion bonding) is a solid state joining process where two components with polished and pre-cleaned surfaces are stacked together and annealed at elevated temperatures to form a bond [61]. Direct bonding causes micro-deformation of surface

features, leading to sufficient contact on an atomic scale to bond different materials. In general, the temperature at which direct bonding will take place, is above one half of the absolute melting temperature of the bonding components. Direct bonding of Si wafers is commonly used in mass production where initial bonding temperatures are between 300 °C and 800 °C then the bonded pairs are annealed at 800-1100 °C to further strengthen the bonds. The high temperature that has been required to achieve acceptable bond strength has been a limitation for direct bonding. Another disadvantage of direct bonding is that, in order to obtain uniform bond, much smoother bonding surfaces are required (surface roughness at a few Angstroms), as compared to anodic bonding (surface roughness at a few 10's nm) [62, 63].

Instead of bonding silicon wafers directly, intermediate layer bonding methods, such as glass frit bonding, thermocompression bonding, eutectic bonding, solder bonding, and adhesive bonding, employ thin films on one or both component surfaces as the bonding media, which help to lower the bonding temperature.

Glass frit bonding is based on the melting of an intermediate low melting point glass film that is screen-printed or sputtered on one or both of the surfaces to be bonded [64]. The bonding temperature depends on the type of glass film used, generally about 400 – 500 ^{o}C. It has been reported that Si anodic bonding can be refined to achieve bonding at low temperature by using a sputtered borosilicate glass with a low melting temperature as a thin film layer on one of the Si surfaces [65-67]. Thermocompression bonding is the joining of two separate surfaces via solid state welding of a layer of soft metals on each surface [68]. The most common metal for silicon wafer bonding is gold. Bonding is

formed by pressing together two wafers with gold pads with applied bonding pressure at elevated temperature. The drawback of this bonding method is the high applied pressure during the bonding process. Solder bonding process works by reflowing low melting point metals to form a bond. Typical solders used in silicon wafer bonding are eutectic PbSn, AgSn, and AuSn [69]. The solder layer can be applied to wafers by screen-printing of solder pastes consisting of small solder spheres, flux, and solvent. The processing temperatures for reflow soldering normally are lower than 250 °C. The problem with solder bonding is that the out-gassing of the flux and solvent in the solder paste during reflow soldering can cause voiding in the bonding area [70]. Eutectic bonding uses Si-Ag, Si-Au, Si-Al, and Au-Sn alloys with eutectic composition as bonding media [71]. The wafers to be bonded are first coated with the two elements of the alloy, such as Si and Au, and then brought into contact. By heating the wafer pair, diffusion occurs at the interface and alloys are formed. The eutectic composition alloy at the interface has a lower melting point than the materials at either side of it, and hence the melting is restricted to a thin layer. It is this melted eutectic layer that forms the bond. Adhesive bonding uses an intermediate adhesive layer such as epoxy to form bonds between two different materials [72]. This bonding process is a simple and inexpensive process and requirements for surface smoothness are low. It can be performed at room temperature or requires only low temperature annealing. The disadvantages of adhesive bonding are long-term instability, a limited working temperature range, low bonding strength, and nonhermeticity of the package. Table 5.1 lists all the wafer bonding techniques mentioned above with their main characteristics.

Table 5.1 Commonly used wafer bonding techniques (Niklaus, 2006)

Wafer bonding technique	Typical bonding conditions	Advantages	Disadvantages
Direct bonding	600-1200 °C Small or no bond pressure	high bond strength; hermetic	high surface flatness; high bond temperature
Anodic bonding	150-500 °C 200-1500 V No bond pressure	high bond strength; hermetic	high voltage
Solder bonding	150-450 °C Low bond pressure	high bond strength; hermetic	solder flux
Eutectic bonding	200-400 °C Low to moderate bond pressure	high bond strength; hermetic	sensitive to native oxide at surfaces
Adhesive bonding	Room temperature up to 400 °C Low to moderate bond pressure	high bond strength; Low bond temperature	low hermetic bonds; Limited temperatures stability

For all of the above bonding methods except for the room temperature adhesive bonding, elevated temperatures are required for bonding silicon wafers. Temperature sensitive

components on the wafers may be damaged or destroyed by the global heating during the bonding process. Dissimilar materials may debond on cooling due to the coefficient of thermal expansion (CTE) mismatch. Thus new approaches with localized heating need to be developed to solve the bonding problem, where high temperature can be locally generated and hermetic and strong bonding can be achieved. At the same time, the temperature outside the bonding area can be kept low.

Localized heating can be produced by embedded microheaters instead of global heating furnaces to prevent thermal problems during bonding [73-76]. These microheaters are constructed in a way that heating is restricted in a small region that is surrounded by insulation materials, such as silicon dioxide. Thus the bonding process can be conducted locally while the whole wafer is maintained at low temperature. However the use of microheaters makes the fabrication and bonding process more complex and time consuming, and heat sinks need to be mounted onto the substrates to release heat from the microheater. Another novel wafer bonding method is localized induction heating solder bonding. Electroplated magnetic Ni/Co film was heated using induction heating that causes the PbSn solder to flow and form a bond [77]. Magnetic induction coil heated up only the magnetic film to high temperature within several seconds and localized heat was realized. The wafer experienced a temperature of only 110 °C during bonding, thus avoiding thermal damage to the devices. However, this method is not suitable to bond devices that are sensitive to magnetic field.

In this study, a novel room temperature bonding technique using reactive multilayer Ni/Al foils as local heat sources to melt solder layers and thus bond silicon wafers was

described. The localized heating and rapid cooling nature made reactive foil joining an ideal method for silicon wafer bonding applications.

5.1 Silicon Wafer Bonding

Using the numerical model developed in Chapter 4, the thickness of reactive foils that can melt the whole solder layer (25 μm) for different joining materials was calculated and listed in Table 5.2. The joining geometry and dimensional parameters are the same as that used for stainless steel in Chapter 4. The thermophysical properties of different materials used in this model were listed in Table 5.3.

Table 5.2 Thickness of reactive foils required to melt the whole solder layer (25 μm) for different joining materials.

Materials	Thickness of foil (μm)
Stainless steel	25
Si	41
Al	48
Cu	86

Ni/Al reactive multilayer foils with Incusil coating (59 wt % Ag-27.25 wt % Cu-12.5 wt % In-1.25 wt % Ti) were used as local heat sources for melting solder layers and joining silicon wafers. According to the simulation results listed in Table 5.2, 60 μm thick Ni/Al foils with bilayer thickness of 40 nm were used. The dimensions of the silicon wafers were 4 inches in diameter and 500 μm in thickness and were coated with Cr (50 nm) and Au (500 nm) by electron-beam evaporation to enhance wetting. These silicon wafers were cut by a diamond blade to a dimension of $25.4\times12.7\times0.5$ mm^3. Two sheets of AuSn

solder (80 wt% Au-20 wt% Sn, Williams Advanced Materials) with thickness of 25 μm and one reactive foil were stacked together between two (100) silicon wafers, as shown schematically in Figure 5.1. Silicon wafer bonding was performed at room temperature in air by igniting the reactive foil under an applied pressure (0.019 MPa). Heat released from the reaction melted the solder layers and thus bonded the silicon wafers together.

Table 5.3 Thermophysical parameters for different joining materials used in the simulation.

	Si	Al	Cu
Thermal conductivity (W/mK)	149	167	388
Heat capacity (J/kgK)	707	896	385
Density (g/cm^3)	2.33	2.70	8.89

All the dimensional parameters of different parts in the silicon wafer bonding are listed in Table 5.4.

Figure 5.2 shows the numerical prediction of temperature evolution within 200 ms at a position 100 μm away from the solder/silicon interface (point A in Figure 5.1) with two 1 cm thick stainless steel substrates. The plot shows that the highest temperature at this position is 164 °C and the temperature decreases to 60 °C after 200 ms. These results

indicate that both localized heating and rapid cooling are achieved by this bonding method.

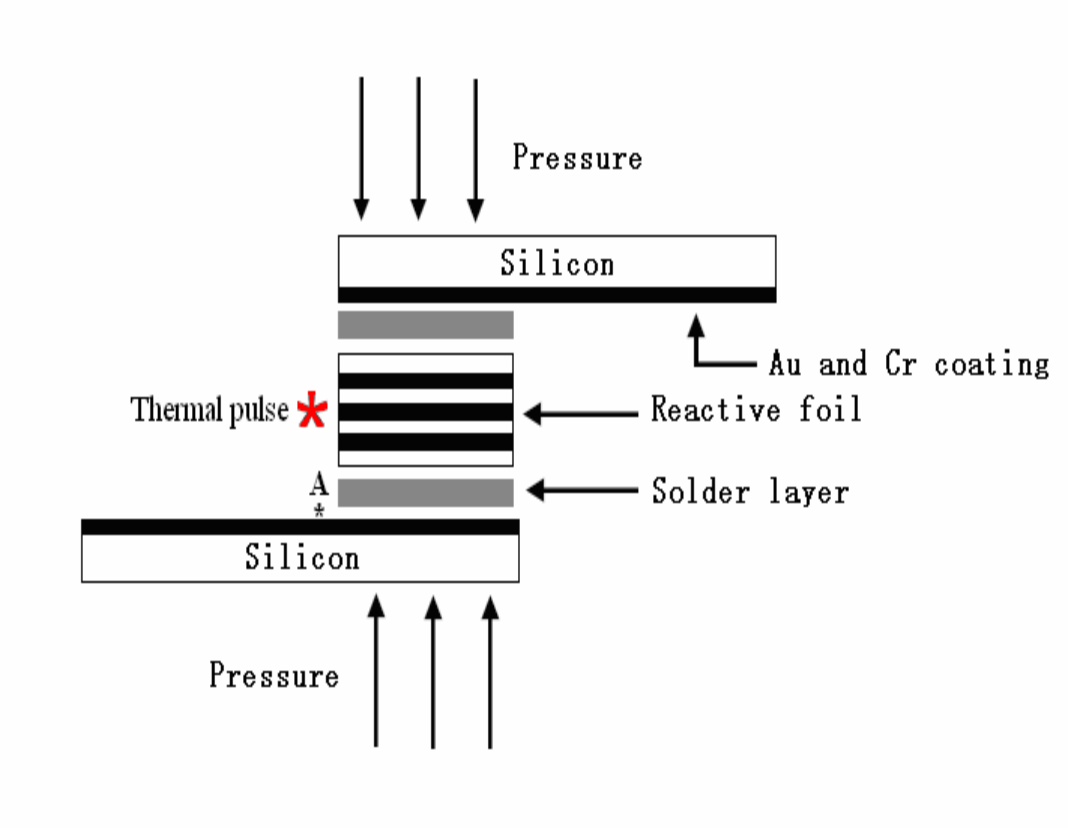

Figure 5.1 Schematic showing the reactive bonding of two silicon wafers using one reactive foil and two solder layers under an applied pressure.

Table 5.4 Dimensional parameters of different parts in silicon wafer bonding.

	Length (mm)	Width (mm)	Thickness (μm)
Si	25.4	12.7	500
Reactive foil	12.7	6.35	60
Solder	5	6.35	25

5.2 Bonding Quality

The bond strength of the silicon wafer joints was examined by pull test. During the test, the sample was fixed between two steel bars by epoxy and then loaded by a mechanical force. Figure 5.3 and 5.4 show the SEM images of the fracture surface of silicon wafer joints. Failure occurred at silicon wafer itself in many regions and silicon was stripped off from one wafer and attached to the other wafer, indicating that the bonding interface is stronger than the silicon wafer itself. The reactive bonding strength is estimated to be larger than the failure strength of bulk silicon at approximately 10 MPa [78].

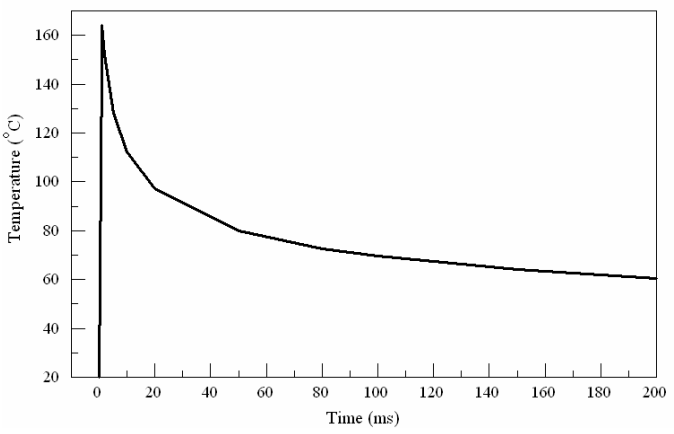

Figure 5.2 Temperature evolutions within 200 ms at a position 100 μm away from the solder/silicon interface.

Figure 5.5 (a) shows two silicon wafers that were bonded using two pieces of free-standing AuSn solder and one Ni/Al reactive foil. Cracking was observed within the reacted foils (Fig 5.5 (b)) and is attributed to the fact that when the foils react they contract due to densification; they also contract due to cooling from the high reaction temperatures. Both sources of contraction can be constrained by the surrounding material, thereby leading to cracking. Molten AuSn solder typically flowed into these cracks, so the solder thickness on the two sides of reactive foils might be different. The

microstructure of the solder/foil interface is shown in Figure 5.6 at a higher magnification. It can be observed that there is intermixing between the solder and the reactive foil at the interface.

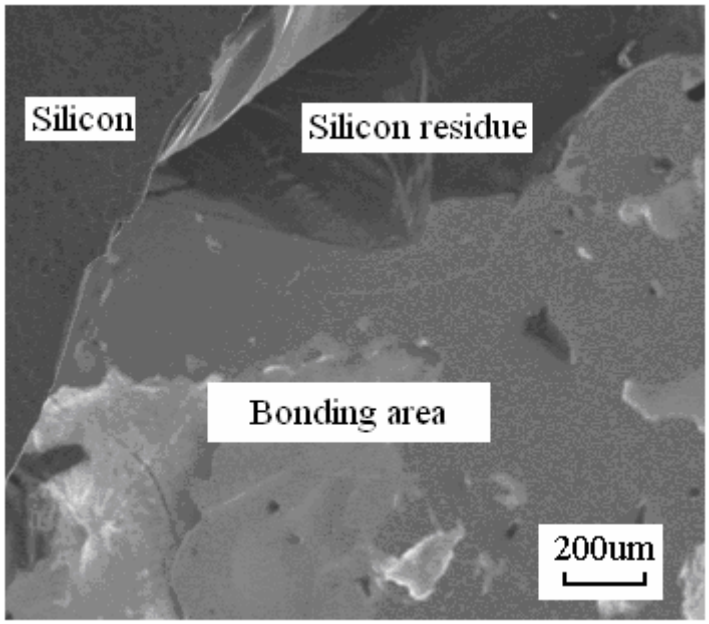

Figure 5.3 Fracture interface of silicon-to-silicon reactive bond.

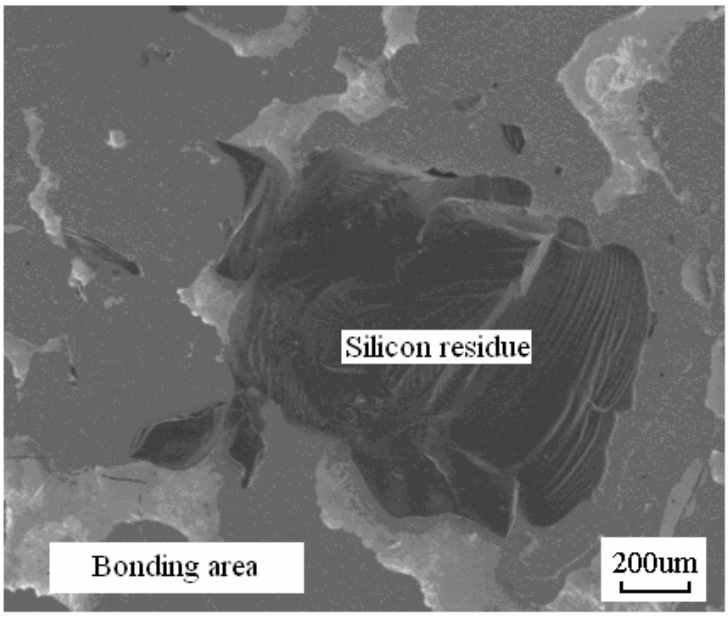

Figure 5.4 Silicon residues on one of the bonded silicon wafers.

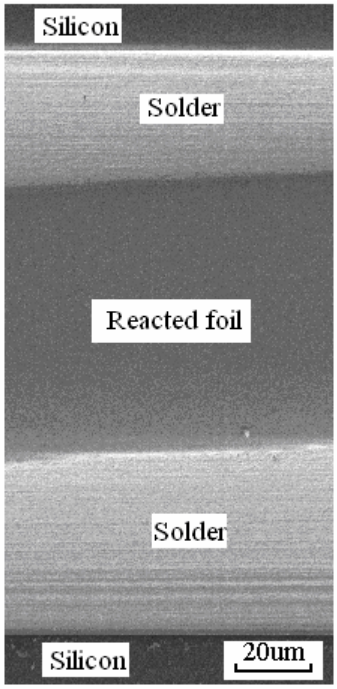

Figure 5.5 (a) SEM micrograph of two silicon wafers that were bonded using two pieces of free-standing AuSn solder and one Ni/Al reactive foil.

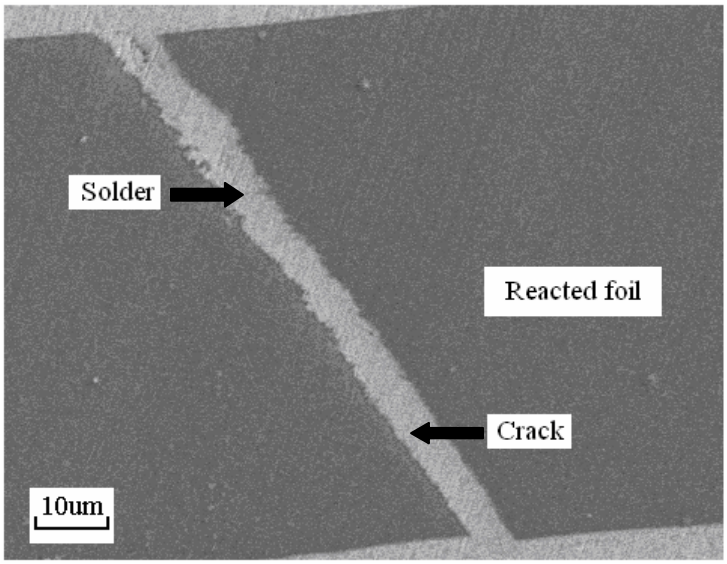

Figure 5.5 (b) Molten solder filled in a crack in the reacted foil formed during the joining process.

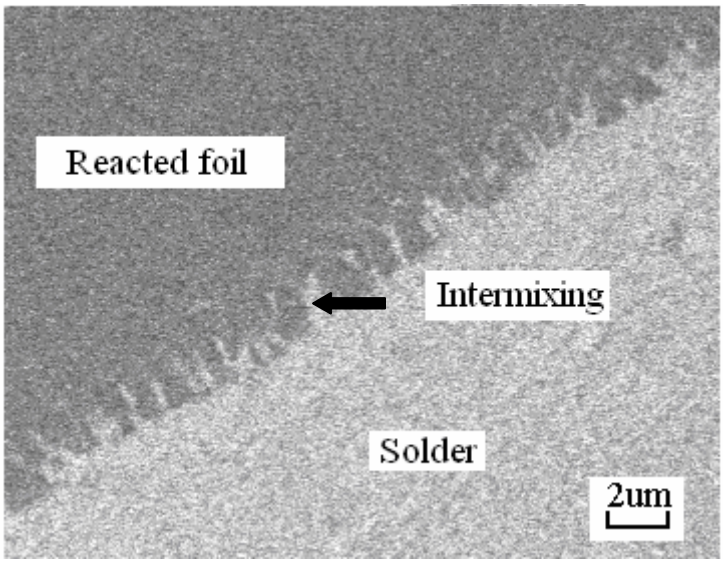

Figure 5.6 The microstructure of the solder/foil interface.

5.3 Leakage Test

A bonded wafer package was immersed in Isopropanol Alcohol (IPA) to conduct the leakage test of liquid. IPA has better wetability than water, and it can more easily penetrate small openings, and therefore is more suitable for leakage test. The bonding geometry of this wafer package is shown in Figure 5.7.

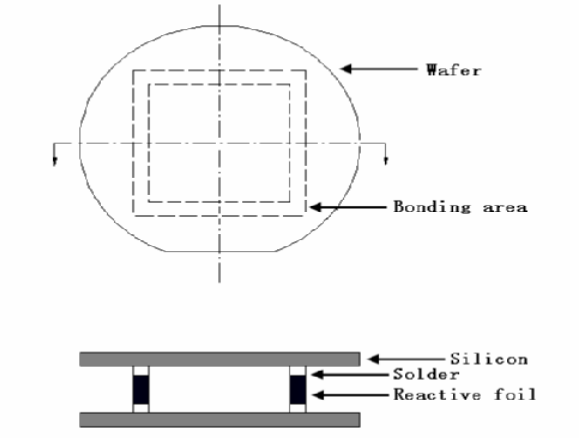

Figure 5.7 Geometry of silicon wafer bonding for leakage test.

The silicon wafers used here are 2 inch diameter (111) silicon wafers with thickness of 300 μm, which was coated with Cr and Au by e-beam evaporation. The area enclosed by the reactive bond is 0.5 inch by 0.5 inch in dimension.

After 12 hours' immersion of the bonded wafer package in IPA, no leakage was detected in the enclosed area. The hermeticiy of the wafer package indicated that this reactive foil bonding approach can be exploited to protect structures enclosed in the package from humidity.

All the experimental results on thermal profiles, bond strength, and hermeticity discussed above indicate that reactive foil joining is an ideal method for silicon wafer bonding and can be used for other general packaging applications.

6. CONCLUSIONS

6.1 Conclusions

1. Ni/Al multilayer foils were fabricated by a cold rolling method. During the ignition experiment, a two-stage reaction process was observed. In stage one, the reaction spread along the lateral direction to the surface of the foil at a relatively slow rate and the foil surface became darker. Then, in stage two, the reaction propagated at a much higher speed and released a large amount of heat, showing visible red light. The final reaction product was AlNi. According to DSC, SEM, and XRD results, the entire reaction process for the cold-rolled Ni/Al multilayer foils can be stated as following. The first reaction stage with a slow reaction velocity was the lateral growth of Al_3Ni phase at isolated nucleation sites and the subsequent coalescence into a continuous layer. The second reaction stage with a fast reaction velocity was the growth of the Al_3Ni layers in the direction normal to the Ni/Al interface until all Al was consumed. Afterwards, Al_3Ni reacted with the remaining Ni to form the final reaction product, AlNi. The reaction velocities of the first reaction stage for the cold rolled foils were around 7 mm/s.

2. Ti/Al multilayer foils were also fabricated by cold rolling to test whether this method can be extended to fabricate other metal/aluminum multilayer systems. According to the SEM and XRD results of the as cold rolled, and the partially reacted Ti/Al multilayer foils, and their reaction products, the entire reaction process for the cold rolled Ti/Al multilayer foils can be identified, which is assumed to be similar to the cold rolled Ni/Al multilayer foils. The first reaction stage was the lateral growth of Al_3Ti phase from isolated nucleation sites and the subsequent coalescence into a

continuous layer. The next reaction stage was the growth of the Al_3Ti layers in the direction normal to the interface until all Al was consumed. Afterwards, Al_3Ti reacted with the remaining Ti to form the final reaction product, AlTi. We have successfully fabricated Ni/Al and Ti/Al multilayer foils by cold rolling. This cold rolling method can be used as a general method to fabricate other metal/Al reactive multilayer foils and can be extended to fabricate other multilayer systems.

3. Silicon wafers were bonded using reactive Ni/Al multilayer foils as local heat sources. A numerical model was developed to predict the temperature evolution during the bonding process. The simulation results showed both localized heating and rapid cooling during reactive joining process, which made reactive foil joining an ideal method for silicon wafer bonding applications. Pull tests were performed for these silicon wafer bonds. The bonds failed at silicon itself, suggesting that the bonding strength is higher than the failure strength of bulk silicon (around 10 MPa). Moreover, leakage test in IPA showed that reactive foil joints possessed good hermeticity for liquid.

6.2 Suggestions for Future Work

1. We have experimentally explored the phase evolutions in cold rolled Ni/Al multilayer foils. The kinetic mechanism for this phase formation process in cold rolled Ni/Al multilayer foils needs to be further studied, such as the activation energy for different reaction stages, and will be compared with Ni/Al multilayers made by physical vapor deposition methods.

2. Reactions in cold rolled Ti/Al multilayer foils needs to be further explored. DSC experiments need to be performed on such foils to reveal the phase evolution process in Ti/Al multilayer foils. The phase formation process in Ti/Al multilayer foils will be compared with the Ni/Al multilayer foils.

3. For the silicon wafer bonding process, reactive foils can be deposited directly on silicon wafers and patterned by lithography process so that this bonding concept can be applied in micropackaging. Both solder bonding and Si-Au eutectic bonding can be performed using the patterned reactive foils. The reactive foils bonding method can be extended to bonding other commonly used materials in packaging, such as Pyrex glass.

REFERENCES

1. J. Subrahmanyam, M. Vijayakumar, "Self-Propagating High-Temperature Synthesis", *J. Mater. Sci*. Vol 27, No 23, 6249-6273, 1992.

2. J. J. Moore, H. J. Feng, "Combustion Synthesis of Advanced Materials I. Reaction Parameters", *Pro. Mater. Sci*. Vol 39, No 4-5, 243-273, 1995.

3. J. J. Moore, H. J. Feng, "Combustion Synthesis of Advanced Materials II. Classification, Applications and Modeling", *Pro. Mater. Sci*. Vol 39, No 4-5, 275-316, 1995.

4. H. C. Yi, J. J. Moore, "Self-Propagating High-Temperature (Combustion) Synthesis (SHS) of Powder-Compacted Materials", *J. Mater. Sci.* Vol 25, No 2B, 1159-1168, 1990.

5. K. Morsi, "Review: Reaction Synthesis Processing of Ni-Al Intermetallic Materials", *Mater. Sci. Eng. A*. Vol 299, No 1-2, 1-15, 2001.

6. A. G. Merxhanov, "Combustion and Plasma Synthesis of High-Temperature Materials", ed Z. A. Munir, J. B. Holt, New York: VCH, 1-53, 1990.

7. L. L. Wang, Z. A. Munir, Y. M. Maximov, "Thermite reactions: their utilization in the synthesis and processing of materials", *J. Mater. Sci.* Vol 28, No 14, 3693-3708, 1993.

8. M. Koizumi, Y. Miyamoto, "Combustion and Plasma Synthesis of High-Temperature Materials", ed Z. A. Munir, J. B. Holt, New York: VCH, 54-60, 1990.

9. T.P. Weihs, "Handbook of Thin film Process Technology", ed D.A. Glocker, S.I. Shah, Institute of Physics, Bristol, UK, F7:1-F7:13, 1998.

10. E. Ma, C. V. Thompson, L. A. Clevenger, K. N. Tu, "Self-propagating explosive reactions in Al/Ni multilayer thin films", *Appl. Phys. Lett.* Vol 57, No 12, 1262-1264, 1990.

11. L. A. Clevenger, C. V. Thompson, K. N. Tu, "Explosive silicidation in nickel/amorphous-silicon multilayer thin films", *J. Appl. Phys.* Vol 67, No 6, 2894-2898, 1990.

12. T. S. Dyer, Z. A. Munir, V. Ruth, "The combustion synthesis of multilayer NiAl systems", *Scripta. Mat*. Vol 30, No 10, 1281-1286, 1994.

13. T. W. Barbee Jr, T. P. Weihs, 1996 US Patent 5538795.

14. D. M. Makowiecki, R. M. Bionta, 1995 US Patent 05381944.

15. D.P. Adams, M.A. Rodriguez, C.P. Tigges, P.G. Kotula, "Self-propagating, high-temperature combustion synthesis of rhombohedral AlPt thin films", *J. Mater. Res.* Vol 21, No 12, 3168-3179, 2006.

16. K. J. Blobaum, M. E. Reiss, J. M. Plitzko Lawrence, T. P. Weihs, "Deposition and characterization of a self-propagating CuO_x/Al thermite reaction in a multilayer foil geometry", *J. Appl. Phys.* Vol 94, No 5, 2915-2922, 2003.

17. T. W. Barbee Jr, T. P. Weihs, 1996 US Patent 5547715.

18. F. Bordeaux, A. R. Yavari, "Ultra rapid heating by spontaneous mixing reactions in metal-metal multilayer composites", *J. Mater. Res.* Vol 5, No 8, 1656-1661, 1990.

19. L. Battezzati, P. Pappalepore, F. Purbiano, I. Gallino, "Solid state reactions in Al/Ni alternate foils induced by cold rolling and annealing", *Acta. Mat.* Vol 47, No 6, 1901-1914, 1999.

20. H. Sieber, J. S. Park, J. Weissmüller, H, Perepezko, "Structural evolution and phase formation in cold-rolled aluminum–nickel multilayers", *Acta. Mat.* Vol 49, No 7, 1139-1151, 2001.

21. C. E. Wickersham Jr, J. E. Poole, "Explosive crystallization in zirconium/silicon multilayers", *J. Vac. Sci. Technol. A.* Vol 6, No 3, 1699-1702, 1988.

22. M. E. Reiss, C. M. Esber, D. Van Heerden, A. J. Gavens, M. E. Williams, T. P. Weihs, "Self-propagating formation reactions in Nb/Si multilayers", *Mater. Sci. Eng. A.* Vol 261, No 1-2, 217-222, 1999.

23. J. Wang, E. Besnoin, A. Duckham, S. J. Spey, M. E. Reiss, O. M. Knio, T. P. Weihs, "Joining of stainless-steel specimens with nanostructured Al/Ni foils", *J. Appl. Phys*. Vol 95, No 1, 248-256, 2004.

24. T. P. Weihs, T. W. Barbee, Jr., M. A. Wall, "A low-temperature technique for measuring enthalpies of formation", *J. Mater. Res.* Vol 11, No 6, 1403-1409, 1996.

25. C Michaelsen, K Barmak, T P Weihs, "Investigating the thermodynamics and kinetics of thin film reactions by differential scanning calorimetry", *J. Phys. D.* Vol 30, No 23, 3167-3186, 1997.

26. J. Wang, E. Besnoin, O. M. Knio, T. P. Weihs, "Effects of physical properties of components on reactive nanolayer joining", *J. Appl. Phys.* Vol 97, No 11, 4307-4313, 2005.

27. J. Wang, E. Besnoin, A. Duckham, S. J. Spey, M. Reiss, O. M. Knio, M. Powers, M. Whitener, T. P. Weihs, "Room-temperature soldering with nanostructured foils", *Appl. Phys. Lett.* Vol 83, No 10, 3987-3989, 2003.

28. A. J. Swiston. Jr, T. C. Hufnagel, T. P. Weihs, "Joining bulk metallic glass using reactive multilayer foils", *Scripta. Mat.* Vol 48, No 12, 1575-1580, 2003.

29. J. Wang, E. Besnoin, O. M. Knio, T. P. Weihs, "Investigating the effect of applied pressure on reactive multilayer foil joining", *Acta. Mat.* Vol 52, No 18, 5265-5274, 2004.

30. A. Duckham, S. J. Spey, J. Wang, M. E. Reiss, T. P. Weihs, "Reactive nanostructured foil used as a heat source for joining titanium", *J. Appl. Phys.* Vol 96, No 4, 2336-2342, 2004.

31. D. Van Heerden, T. Rude, J. Newson, O. Knio, T. P. Weihs, "Thermal Behavior of a Soldered Cu-Si interface", 20th IEEE SEMI-THERM Symposium, 2004.

32. T. Namazu, H. Takemoto, H. Fujita, Y. Najai, S. Inoue, "SELF-PROPAGATING EXPLOSIVE REACTIONS IN NANOSTRUCTURED AL/NI MULTILAYER FILMS AS A LOCALIZED HEAT PROCESS TECHNIQUE FOR MEMS", IEEE MEMS 2006, Istanbul, Turkey, 2006.

33. E. G. Colgan, "A review of thin-film aluminide formation", *Mater. Sci. Rep.* Vol 5, No 1, 1-44, 1990.

34. E. Ma, C. V. Thompson, L. A. Clevenger, "Nucleation and growth during reactions in multilayer Al/Ni films: The early stage of Al_3Ni formation", *J. Appl. Phys.* Vol 69, No 4, 2211-2218, 1991.

35. A. S. Edelstein, R. K. Everett, G. Y. Richardson, S. B. Qadri, E. I. Altman, J. C. Foley, J. H. Perepezko, "Intermetallic phase formation during annealing of Al/Ni multilayers", *J. Appl. Phys.* Vol 76, No 12, 7850-7859, 1994.

36. A. S. Edelstein, R. K. Everett, G. Y. Richardson, S. B. Qadri, E. I. Altman, J. C. Foley, J. H. Perepezko, "Reaction kinetics and biasing in Al/Ni multilayers", *Mater. Sci. Eng. A.* Vol 195 No 6, 13-19, 1995.

37. K. J. Blobaum, D. Van Heerden, A. J. Gavens, T. P. Weihs, "Al/Ni formation reactions: characterization of the metastable Al_9Ni_2 phase and analysis of its formation", *Acta. Mat.* Vol 51, No 13, 3871-3884, 2003.

38. C. Michaelsen, G. Lucadamo, K. Barmak, "The early stages of solid-state reactions in Ni/Al multilayer films", *J. Appl. Phys.* Vol 80, No 12, 6689-6698, 1996.

39. K. Barmak, C. Michaelsen, G. Lucadamo, "Reactive phase formation in sputter-deposited Ni/Al multilayer thin films", *J. Mater. Res.* Vol 12, No 1, 133- 146, 1997.

40. K. R. Coffey, L. A. Clevenger, K. Barmak, D. A. Rudman, C. V. Thompson, "Experimental evidence for nucleation during thin-film reactions", *Appl. Phys. Lett.* Vol 55, No 9, 852-854, 1989.

41. R. Pretorius, A. M. Vredenberg, F. W. Saris, R. de Reus, "Prediction of phase formation sequence and phase stability in binary metal-aluminum thin-film systems using the effective heat of formation rule", *J. Appl. Phys.* Vol 70, No 7, 3636-3646, 1991.

42. J.M. Rickman, W.S. Tong, K. Barmak, "Impact of heterogeneous boundary nucleation on transformation kinetics and microstructure", *Acta. Mat*. Vol 45, No 3, 1153-1166, 1997.

43. K. Barmak, J.M. Rickman, C. Michaelsen, "Evolution of Grain Structure in Thin Film Reactions", *J. Electron. Mater.* Vol 26, No 9, 1009-1020, 1997.

44. A. B. Mann, A. J. Gavens, M. E. Reiss, D. Van Heerden, G. Bao, T. P. Weihs, "Modeling and characterizing the propagation velocity of exothermic reactions in multilayer foils", *J. Appl. Phys.* Vol 82, No 3, 1178-1188, 1997.

45. A. J. Gavens, D. Van Heerden, A. B. Mann, M. E. Reiss, T. P. Weihs, "Effect of intermixing on self-propagating exothermic reactions in Al/Ni nanolaminate foils", *J. Appl. Phys.* Vol 87, No 3, 1255-1263, 2000.

46. F. J. J. Van Loo, G. D. Rieck, "Diffusion in the Ti-Al System. I. Interdiffusion between Solid Al and Ti or Ti-Al", *Acta. Mat*. Vol 21, No 1, 61-71, 1973.

47. R. W. Bower, "Characteristics of aluminum-titanium electrical contacts on silicon", *Appl. Phys. Lett.* Vol 23, No 2, 99-101, 1973.

48. G. Lucadamo, K. Barmak, C. Lavoie, C. Cabral. Jr, C. Michaelsen, "Metastable and equilibrium phase formation in sputter-deposited Ti/Al multilayer thin films", *J. Appl. Phys.* Vol 91, No 12, 9575-9583, 2002.

49. William. D. Callister. Jr, "MATERIALS SCIENCE AND ENGINEERING AN INTRODUCTION", 7th edition, WILEY, 2007.

50. G. Lucadamo, K. Barmak, S. Hyun, C. Cabral Jr., C. Lavoie, "Evidence of a two-stage reaction mechanism in sputter deposited Nb/Al multilayer thin-films studied by in situ synchrotron X-ray", *Mater. Lett.* Vol 39, No 5, 268-273, 1999.

51. X. Sauvage, G.P. Dinda, G. Wilde, "Non-equilibrium intermixing and phase transformation in severely deformed Al/Ni multilayers", *Scripta. Mat.* Vol 56, No 3, 181-184, 2007.

52. A.J. Swiston. Jr, E. Besnoin, A. Duckham, O.M. Knio, T.P. Weihs, T.C. Hufnagel, "Thermal and microstructural effects of welding metallic glasses by self-propagating reactions in multilayer foils", *Acta. Mat*. Vol 53, No 13, 3713-3719, 2005.

53. Xiaotun Qiu, Jiaping Wang, "Reactive Multilayer Foils for Silicon Wafer Bonding", *Mater. Res. Soc. Symp. Proc.* Vol 968, V02-06, 2007.

54. www. cocoe. sourceforge. net

55. L. Gardner, K. T. Ng, "Temperature development in structural stainless steel sections exposed to fire", *J. Fire. Safety.* Vol 41, No 3, 185-203, 2006.

56. M. A. Schmidt, "Wafer-to-Wafer Bonding for Microstructure Formation", *Proc. IEEE.* Vol 86, No 8, 1575-1585, 1998.

57. K. M. Knowles, A. T. J. Van Helvoort, "Anodic bonding", *Int. Mater. Rev.* Vol 51, No 5, 273-311, 2006.

58. C. H. Tsau, S. M. Spearing, M. A. Martin, "Characterization of Wafer-level Thermocompression Bonds", *J. MEMS.* Vol 13, No 6, 963-971, 2004.

59. F. Niklaus, G. Stemme, J. Q. Lu, R. J. Gutmann, "Adhesive wafer bonding", *J. Appl. Phys.* Vol 99, No 3, 1101-1128, 2006.

60. G. Wallis, D. I. Pomerantz, "Field Assisted Glass-Metal Sealing", *J. Appl. Phys.* Vol 40, No 10, 3946-3949, 1969.

61. P. W. Barth, "Silicon Fusion Bonding for Fabrication of Sensors, Actuators and Microstructures", *Sensors and Actuators A*. Vol 23, No 1-3, 919-926, 1990.

62. C. Harendt, C. E. Hunt, W. Appel, H. Graf, B. Hofflinger, E. Penteker, "Silicon on Insulator Material by Wafer Bonding", *J. Electron. Mater.* Vol 20, No 3, 267-277, 1991.

63. W. P. Maszara, G. Goetz, A. Caviglia, J. B. McKittereck, "Bonding of Silicon Wafers for Silicon on Insulator", *J. Appl. Phys.* Vol 64, No 10, 4943-4950, 1988.

64. R. Knechtel, M. Wiemer, J. Fromel, "Wafer Level Encapsulation of Microsystems using Glass Frit Bonding", *Microsyst. Technol.* Vol 12, No 5, 468-472, 2006.

65. W. B. Choi, B. K. Ju, Y. H. Lee, J. W. Jeong, M. R. Haskards, N. Y. Lee, M. Y. Sung, M. H. Oh, "Experimental Analysis of the Anodic Bonding with an Evaporated Glass Layer", *J. Micromech. Microeng.* Vol 7, No 4, 316-322, 1997.

66. S. Weichel, R. Reus, M. Lindahl, "Silicon-to-silicon Anodic Wafer Bonding using Evaporated Glass", *Sensors and Actuators A*. Vol 70, No 1-2, 179-184, 1998.

67. A. Hanneborg, M. Nese, P. Ohlckers, "Silicon-to-silicon Anodic Bonding with a Borosilicate Glass Layer", *J. Micromech. Microeng.* Vol 1, No 3, 139-144, 1991.

68. M. M. V. Taklo, P. Storas, K. Schjolberg-Henriksen, H. K. Hasting, H. Jakobsen, "Strong, High-yield and Low-temperature Thermocompression Silicon Wafer-level Bonding with Gold", *J. Micromech. Microeng.* Vol 14, No 7, 884-890, 2004.
69. A. Goyal, J. Cheong, S. Tadigadapa, "Tin-based Solder Bonding for MEMS Fabrication and Packaging Applications", *J. Micromech. Microeng.* Vol 14, No 6, 819-825, 2004.

70. D. Sparks, G. Queen, R. Weston, G. Woodward, M. Putty, L. Jordan, S. Zarabadi, K. Jayakar, "Wafer-to-wafer Bonding of Nonplanarized MEMS Surfaces using Solder", *J. Micromech. Microeng.* Vol 11, No 6, 630-634, 2001.

71. Y. Mei, G. R. Lahiji, K. Najafi, "A Robust Gold-Silicon Eutectic Wafer Bonding Technology for Vacuum Packaging", Tech. Dig. Solid-State Sensor and Actuator Workshop. 2002.

72. F. Sarvar, D. A. Hunt, D. C. Whalley, "Application of Adhesives in MEMS and MOEMS Assembly: A Review", *Proc. IEEE Polytronic*. 22-28, 2002.

73. Y. T. Cheng, W. T. Hsu, K. Najafi, T. C. Nguyen, L. Lin, "Vacuum Packaging Technology using Localized Aluminum/Silicon-to-glass Bonding", *J. MEMS.* Vol 11, No 5, 556-565, 2002.

74. Y. T. Cheng, L. Lin, K. Najafi, "A Hermetic Glass-Silicon Package Formed Using Localized Aluminum/Silicon-Glass Bonding", *J. Micromech. Microeng.* Vol 10, No 3, 392-399, 2001.

75. A. Cao, M. Chiao, L. Lin, "Selective and Localized Wafer Bonding using Induction Heating", Technical Digest of Solid-State Sensors and Actuators Workshop. 2002.

76. Y. T. Cheng, L. Lin, K. Najafi, "Localized Silicon Fusion and Eutectic Bonding for MEMS Fabrication and Packaging", *J. MEMS.* Vol 9, No 1, 3-8, 2000.

77. H. Yang, M. Wu, W. Fang, "Localized Induction Heating Solder Bonding for Wafer Level MEMS Packaging", *J. Micromech. Microeng.* Vol 15, No 2, 394-399, 2005.

78. Robert W. Bower, Mohd S. Ismail, Brian E. Roberds, "Low temperature Si_3N_4 direct bonding", *Appl. Phys. Lett.* Vol 62, No 26, 3485-3487, 1993.

79. X. Qiu, J. Wang, "Experimental evidence of two-stage formation of Al_3Ni in reactive Ni/Al multilayer foils", *Scripta. Mat.* Vol 56, No 12, 1055-1058, 2007.

80. X. Qiu, J. Graeter, L. Kecskes, J. Wang, "Exothermic Reactions in Cold Rolled Ni/Al Reactive Multilayer Foils", submitted to *J. Mater. Res.*

81. X. Qiu, J. Graeter, L. Kecskes, J. Wang, “Fabrication and Characterization of Cold Rolled Ni/Al Multilayer Foils”, *Mater. Res. Soc. Symp. Proc.* Vol 977E, FF01-02, 2007.

VITA

Xiaotun Qiu was born in September 1981, in Bei An, Heilongjiang Province, China. He received a degree of Bachelor of Science in Mechanical Engineering from Department of Precision Instruments and Mechanology, Tsinghua University, China, in 2004. Then he worked there as a research associate till December 2005.

In January 2006, he joined the Mechanical Engineering Department at Louisiana State University, Baton Rouge, to pursue his Master of Science in Mechanical Engineering degree. He expects to receive that degree in summer 2007.